UNIVERSIDAD NACIONAL DE INGENIERÍA
FACULTAD DE CIENCIAS

SECCIÓN DE POSGRADO Y SEGUNDA ESPECIALIZACIÓN PROFESIONAL

CELDAS SOLARES FOTOELECTROQUÍMICAS DE DIÓXIDO DE TITANIO SENSIBILIZADAS Y MODIFICADAS CON ALUMINIO

TESIS

PARA OBTENER EL GRADO DE:

DOCTOR EN CIENCIAS

MENCIÓN EN QUÍMICA

PRESENTADA POR:

HUGO ARTURO ALARCÓN CAVERO

LIMA – PERÚ

2008

CONTENTS

PREFACE

The work presented in this thesis was carried out at the Department of Physical Chemistry, Uppsala University and at the Department of Center Molecular Devices, Royal Institute of Technology (KTH) in Sweden and at the Laboratory Thin Films of the Universidad Nacional de Ingeniería in Perú during the years 2002 – 2006 under the main supervision of the Dr. Anders Hagfeldt from Sweden and the Dr. Walter Estrada from Peru. Most the experimental work was performed in Sweden.

This doctoral thesis was made as a cooperative program between the Uppsala University and the Royal Institute of Technology - Sweden and the Universidad Nacional de Ingeniería- Peru.

The subject is photoelectrochemical, this thesis present the efficiency optimization and optoelectrical characterization of dye –sensitized solar cells based on TiO_2 coated with aluminum oxide. The main application considered was for energy conversion.

This thesis is based on the following papers.

I. ***Dye- Sensitized Solar Cells based on nanocrystalline TiO_2 films surface treated with Al^{+3} ions: photovoltage and electron transport studies***

H. Alarcón, G. Boschloo, P. Mendoza, J.L. Solis and A. Hagfeldt

J. Phys. Chem. B 2005, 109, 1843-18490

II. Modification of Nanostructure TiO_2 electrodes by electrochemical Al^{+3} insertion: Effects on Dye-Sensitized Solar Cells performance

Hugo Alarcón, M.Hedlund, Erik Johanson, H. Rensmo, A. Hagfedlt and G. Boschloo

J. Phys. Chem. C. 2007, 111, 13267-13274

Acknowledgment

First to all, I would like to express my gratitude to my supervisors Anders Hagfeldt in Sweden and Walter Estrada in Perú for the support and believing in me.

I wish to thank to all people of Department of Physical chemistry, Uppsala University and of the Department of Center Molecular Devices (KTH) for creating pleasant working atmosphere, in especial to Leif, Tannia, Gema, Tomas, Teresa and Gerrit Boschloo my co-supervisor.

I wish to tank to the people from Faculty of Science of the Universidad Nacional de Ingeniería, to all the members of thin films group: Yuri, Abel, Juan, Jose, Clemente, Luis and especially to Monica for her support to my doctoral studies.

I am also grateful to Malin Akerblom and all staff at ISP for their constant help in my stay in Sweden.

I gratefully acknowledge all co-authors Maria Hedlund, Erik Johanson, Håkan Rensmo and Jose Solis.

My gratitude to my family especially my parents Hugo and Josefina, and my sister Miriam and my brother Alfredo, for help me and be with me in all moment.

I would like to give especially thank to Sarita my wife, for make my life happy and love me in all moment.

This work was carried out at the Department of Physical Chemistry, Uppsala University and at the Department of Center Molecular Devices, Royal Institute of Technology (KTH) in Sweden. It was financially supported by the International Science Programs in Chemistry of Uppsala University

ABSTRACT

This work presents two ways of modifying the surface of TiO_2 with Al^{3+}, the first way was made by depositing a TiO_2 suspension containing small amounts of aluminum nitrate or aluminum chloride onto conducting glass substrates, followed by drying, compression, and finally heating to 530 °C. Electrodes prepared with TiO_2 nanoparticles coated with less than 0.3 wt % aluminum oxide with respect to TiO_2 improved the efficiency of the dye sensitized solar cell. This amount corresponds to less than a monolayer of aluminum oxide. Thus, the Al ions terminate the TiO_2 surface rather than form a distinct aluminum oxide layer. The aluminum ion surface treatment affects the solar cell in different ways: the potential of the conduction band is shifted, the electron lifetime is increased, and the electron transport is slower when aluminum ions are present between interconnected TiO_2 particles.

The second way was made by insertion of aluminum ions using an electrochemical process. After heat treatment these films were found suitable as electrodes in dye-sensitized solar cells. By means of a catechol adsorption test, as well as photoelectron spectroscopy (PES), it was demonstrated that the density of Ti atoms at the metal oxide/electrolyte interface is reduced after Al modification. There is, however, not a complete coverage of aluminum oxide onto the TiO_2, but the results rather suggest either the formation of a mixed Al-Ti oxide surface layer or formation of a partial aluminum oxide coating. No new phase could, however, be detected. In solar cells incorporating Al-modified TiO_2 electrodes, both electron lifetimes and electron transport times were increased. At high concentrations of inserted aluminum ions, the quantum efficiency for electron injection was significantly decreased.

Results are discussed at the hand of different models: A multiple trapping model, which can explain slower kinetics by the creation of additional traps during Al insertion, and a surface layer model, which can explain the reduced recombination rate, as well as the reduced injection efficiency, by the formation of a blocking layer.

Abbreviations

α	absorption coefficient or cathodic transfer coefficient (cm^{-1}).
c	concentration (mol dm^{-3}).
d	film thickness (cm)
D_0	diffusion coefficient of free electrons ($cm^2\ s^{-1}$).
D_n	apparent (trap controlled) electron diffusion coefficient ($cm^2\ s^{-1}$).
$\Delta\phi$	potential difference across space charge region of a semiconductor (V).
E	electrode potential (V) or energy (eV).
E^0	standard electrode potential (V).
E_c	conduction band energy (eV).
E_F	Fermi energy (eV)
${}_nE_F$	quasi Fermi energy (eV).
$E_{F,redox}$	redox Fermi energy (eV).
ε_0	permittivity of vacuum ($F\ cm^{-1}$).
f_{FD}	Fermi Dirac function (dimensionless).
FF	fill factor (dimensionless).
ϕ	electrostatic potential (V).
$g(E)$	density of states function for electron traps ($cm^{-3}\ eV^{-1}$).
η	overpotential for an electrode process (V).
η_{inj}	injection efficiency of sensitization process.
I_0	incident photon flux ($cm^{-2}\ s^{-1}$)
j	current density ($A\ cm^{-2}$)

j^0	exchange current density for an electrode reaction (A cm^{-2}).
$j_{lim,a}$	diffusion limited anodic current density (A cm^{-2}).
$j_{lim,c}$	diffusion limited cathodic current density (A cm^{-2}).
j_{photo}	photocurrent density (A cm^{-2}).
j_{sc}	short circuit current density (A cm^{-2}).
j_{sub}	current density at substrate.
j^0_{sub}	exchange current density at substrate.
J_i	flux of species *i* (cm^{-2} s^{-1}).
k	rate constant for a volume process (s^{-1}).
k_B	Boltzmann constant (eV K^{-1}).
L_n	electron diffusion length (cm).
λ	wavelength (nm).
$\bar{\mu}_i$	electrochemical potential of species *i*.
μ_i^0	standard chemical potential of species *i*.
n_c	conduction band electron density (cm^{-3}).
n^0_c	equilibrium (dark) conduction band electron density (cm^{-3}).
n_i	number density of particles *i* (cm^{-3}).
n_t	density of trapped electrons (cm^{-3}).
N_d	donor density (cm^{-3}).
q	elementary charge (C).
T	absolute temperature (K).
τ_0	conduction band electron lifetime (s).
τ_n	electron lifetime (s).

U	voltage (V).
U_{photo}	photovoltage (V).
υ	volume rate of a process ($cm^{-3}\ s^{-1}$).
V_{oc}	open circuit voltage (V).
z	number of electrons transferred in an electrode reaction.

CHAPTER I

1. INTRODUCTION

1.1 Objectives

The purpose of this work is the preparation of dye- sensitized solar cells with nanoparticles of TiO_2 modified with aluminum for improve the efficiency of these kinds of devices, this way will contribute to the research for better and cheaper materials for solar conversion applications. This type of solar cells presents good advantages: it gives higher conversion efficiencies at lower of light intensity than conventional solar cells, it is easy to fabricate without demanding expensive materials.

1.2 Overview

The generation of electricity from sunlight at large scale and low cost be not far from reality in this century. Rapidly emerging solar energy technologies use low cost dye sensitized photovoltaic cell. Though the silicon solar cell are more efficient in converting solar energy into electricity until now, the non-conventional solar cell based on molecular photosensitization by colored materials on wide band gap semiconductors is a fast growing field of basic scientific and industrial research. The solar cells using molecular dyes shows energy conversion with efficiencies of 10- 11%.[1,2]

Dye-sensitized solar cell (DSSC) is a new and interesting alternative solar cell technology that has received much attention in recent years.[3-5] A typical DSC comprises a dye sensitized porous nanostructured TiO_2 film interpenetrated by a liquid electrolyte containing the iodine/iodide redox couple. A convenient method to prepare nanostructured TiO_2 films is the compression method: a TiO_2 powder film on a substrates is compressed using a pressure of about 500 – 1000 kg cm^{-2}. [6,7]

In efficient DSSC devices the possible recombination pathways occurring at the TiO_2/dye/electrolyte interface should be minimized, allowing charge collection at the device contacts. It has been reported that the DSC´s efficiency can be improved by surface modification of TiO_2 by insulating

oxides or high band gap semiconductors that form a blocking layer between the dye sensitizer and the semiconductor oxide.[8-11]

The electron injection from the excited state of the dye into the conduction band of the TiO_2 can occur by tunneling through the very thin insulating oxide.[12] The thickness of the insulating oxide must be thin enough to allow the passage of electrons by tunneling; otherwise it will decrease the efficiency of the solar cell. The injected electron may recombine at the solid-liquid interface, either with oxidized dye molecules or with the oxidized redox couple. The insulating oxide layer can reduce the interfacial recombination.

There are several studies in which a thin layer of an insulating or wide-bandgap oxide was added to the nanostructured metal oxide to improve the performance of DSSC.[8-13] For example, the efficiency of DSSC based on TiO_2 and SnO_2 was improved by thin layers of Al_2O_3, Nb_2O_5 and MgO.[9-13] It has been shown that Al_2O_3, ZrO_2 and SiO_2 overlayers on TiO_2 act as barrier layers for interfacial electron transfer processes.[12]

Several methods have been applied to deposit thin insulates oxides: dip-coating in metal alkoxide solutions,[9,10,12] chemical vapor deposition,[14] and mixing of metal salts like $AlCl_3$ and $Al(NO_3)_3$ with TiO_2 or SnO_2 nanoparticles in solution followed by annealing.[10,11,13] Recently, an electrochemical modification of nanostructured TiO_2 using electrochemical deposition of the hydroxides of Mg, Zn, Al, and La was described.[15]

Scheme 1, shows the photogeneration of the dye excited state (a), the electron injection into the conduction band of nanoporous TiO_2 (b), the regeneration of the dye ground state by electron transfer from the redox couple (c), the charge recombination pathways of the injected electron with oxidized dye molecules (d) and with oxidized redox couple (e), and finally dye excited state decay to ground (f).[12]

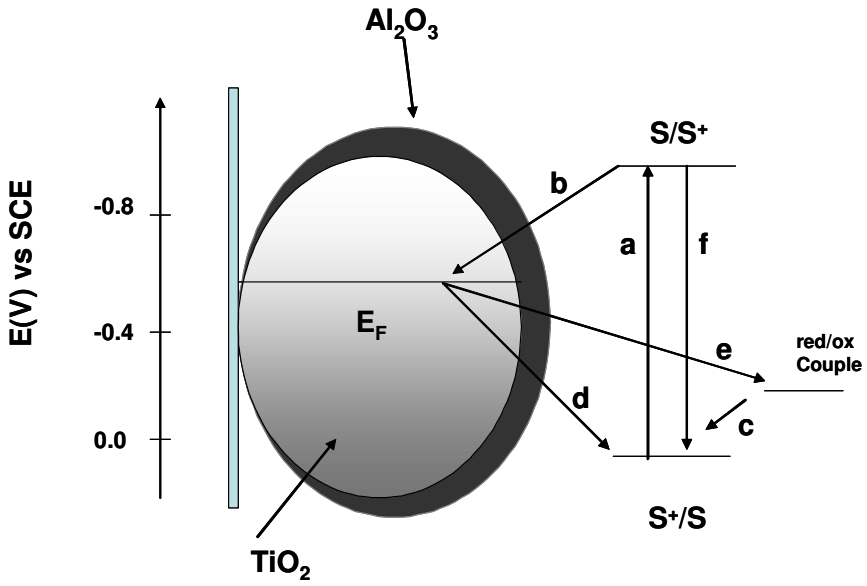

Scheme 1. *Schematic representation of Electron Transfer process in dye – sensitize blocking layer photoelectrode.*

This work presents two ways of modifying the surface of TiO_2 with aluminum. A very simple method is to mix metal salts into the TiO_2 suspension, so that a metal oxide coating is formed upon sintering.[10] The advantage of this method is that the amount of insulating metal oxide can be controlled accurately.

The other method consists in using an electrochemical process in which good control of the amount of aluminum incorporated in the film of TiO_2 is obtained. It is well known that small cations, such as Li^+ and Na^+, can intercalate reversibly into TiO_2 electrodes when a negative potential is applied[16,17] It was shown recently that Li-intercalation can give marked effects on the characteristics of TiO_2-based DSSC.[18]

The electrochemical incorporation of Al^{3+} into TiO_2 was found to be highly irreversible. In both cases, present the Optoelectrical characterization of the aluminum-modified TiO_2 dye-sensitized solar cells is presented. The overall effect was a modest improvement of the solar cell efficiency.

1.2.1 Photovoltaic Cell Performance

A photovoltaic cell is a device that converts incident light into electrical energy.

Generation of electrical power under illumination is achieved by the capability of the photovoltaic device to produce voltage over an external load, and current through the load at the same time. This is characterized by the current-voltage (IV) curve of the cell at certain illumination and temperature (Figure 1).

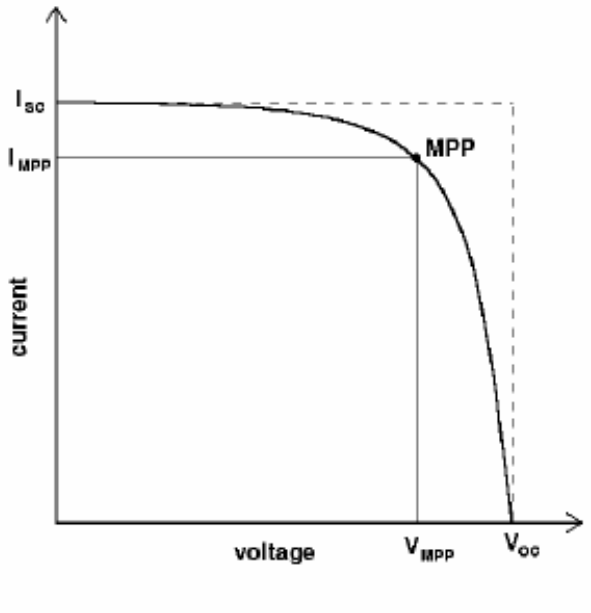

Figure1. *Typical shape of the current-voltage curve of a photovoltaic cell showing the open circuit voltage V_{OC}, short circuit current I_{SC}, and the maximum power point MPP, and the current and voltage at the MPP: I_{MPP}, V_{MPP}.*

When the cell is short circuited under illumination, the maximum current, the short circuit current (I_{SC}), is generated, while under open circuit conditions no current can flow and the voltage is at its maximum, called the open circuit voltage (V_{OC}). The point in the IV-curve yielding maximum product

of current and voltage, i.e. power, is called the maximum power point (MPP). Another important characteristic of the solar cell performance is the fill factor (FF), defined as:

$$FF = \frac{V_{MPP}.I_{MPP}}{V_{OC}.I_{SC}} \quad \text{.....(1)}$$

Using the fill factor, the maximum power output of the solar cell can be written as:

$$P_{MAX} = V_{OC}.I_{SC}.FF \quad \text{..... (2)}$$

While the physical principles behind the operation of different types of photovoltaic cells are generally different, the current-voltage curve of well performing cells are similar, and can be characterized and compared with each other in terms of FF, V_{OC}, and I_{SC}.

Finally, the energy conversion efficiency of the solar cell is defined as the power produced by the cell (P_{MAX}) divided by the power incident on the representative area of the cell (P_{light}):

$$\eta = \frac{P_{MAX}}{P_{light}} \quad \text{.....(3)}$$

The efficiency of the solar cell depends on the temperature of the cell, and what is even more important, on the quality of the illumination, i.e. the total light intensity and the spectral distribution of the intensity. For this reason, a standard measurement condition has been developed to facilitate comparable testing of the solar cells between different laboratories.

In the standard condition used for testing of terrestrial solar cells the light intensity is 1000 W/m^2, the spectral distribution of the light source is that

of AM1.5 global standard solar spectrum (Figure 2), and temperature of the cell is 25°C. The power output of the solar cell at these conditions is the nominal power of the cell, or module, and is reported in *peak* watts, Wp. In practice, special solar simulator light sources are used for the standard measurements.

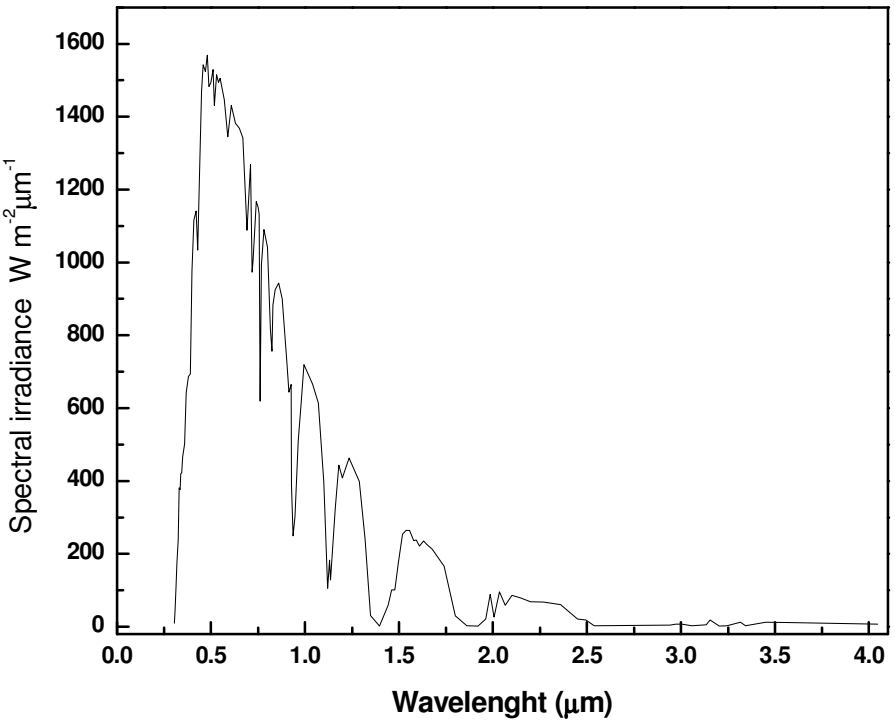

Figure 2. *The standard AM1.5 global solar spectrum*

1.2.2 Standard silicon solar cell

The standard silicon solar cell is based on a semiconductor pn-junction. The cell consists of n-doped and p-doped semiconductor layers forming the pn-junction, an antireflection coating, current collectors and a

metal substrate for the collection of photogenerated charge carriers from n-type (electrons) and p-type (holes) layers, respectively.

n-type semiconductors are obtained by doping with impurity atoms (from group V in the case of silicon) having an excess valence electron with respect to the surrounding host atoms. p-type semiconductors on the other hand are obtained by doping with impurity atoms (from group III in the case of silicon) with one valence electron less than the surrounding atoms. The n-type doping results in localized energy states just below the conduction band edge of the host semiconductor lattice and occupied by the excess electrons from the impurity atoms, while p-type doping results in (Figure 3) localized empty states with energy slightly above the valence band edge of the semiconductor.

The donor atoms in the n-type material are easily ionized by thermal excitation, due to the closeness of the donor states and the conduction band edge. The ionization of the donor atoms generates free electrons to the conduction band and leaves immobile empty donor states behind. For the same reason in the p-type material the originally empty acceptor states are partly filled by electrons from the valence band leaving mobile holes to the valence band.

Bringing an n-type and p-type semiconductor in contact leads to a transport of electrons and holes across the junction until equilibrium is reached. This can be described as equalization of the Fermi-level in the both materials in thermal equilibrium with each other, and this process sets up a depletion zone near the junction where there are practically no free charges, but an electric field (potential difference) across the region.

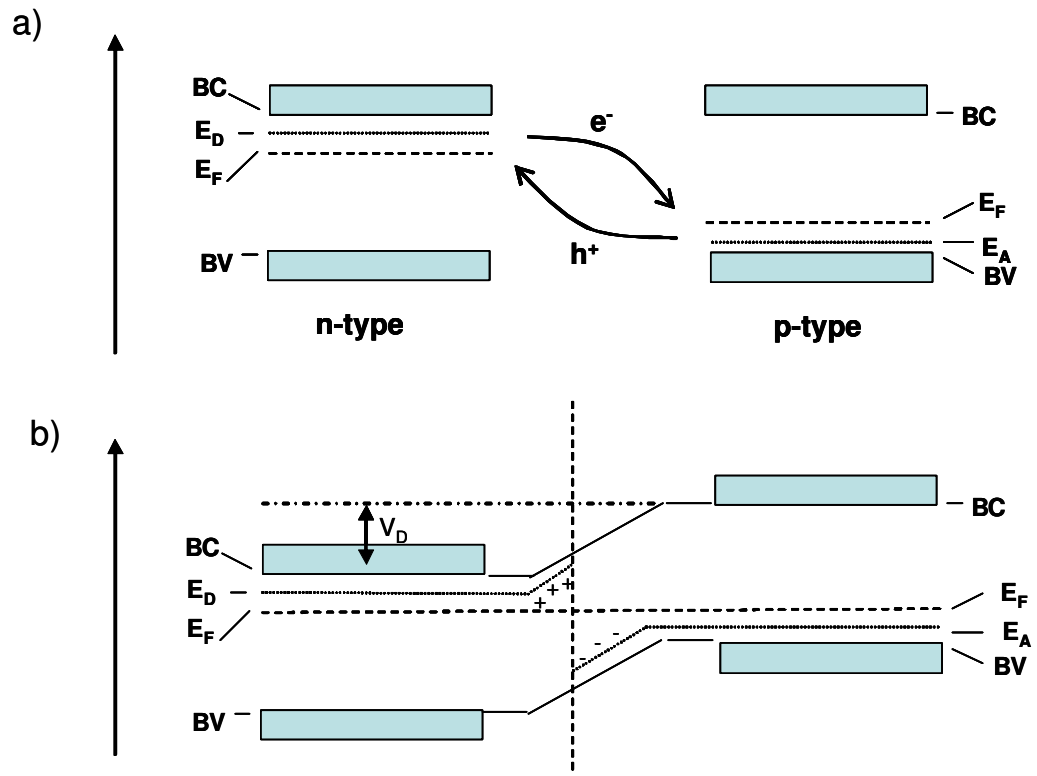

Figure 3. *Formation of the semiconductor pn-junction. a) Schematic band structure of an n-type and a p-type semiconductor showing conduction and valence band edges BC and BV, donor level E_D in n-type material and acceptor level E_A in the p-type material and the Fermi level E_F. b) pn-junction in thermal equilibrium has the potential difference V_D across the junction.*

The operation of a photovoltaic cell can be generally divided into three basic steps:

1. Light absorption,
2. Charge separation,
3. Charge collection.

The physical or chemical processes behind these principal steps vary among different types of solar cells and photovoltaic materials. The efficiency

of a solar cell depends on the efficiency of each of these steps and is maximized by the materials selection and the cell design.

1.2.3 Dye sensitized solar cell (DSSC)

E. Bequerel the first to discover the conversion of light into electricity in 1839. He observed the generation of electricity when two electrodes were put a conducting solution and exposed to light. In the 19th century many others materials, including silicon, that convert light into electric energy were discovered. At the beginning the efficiency was low, but at the present time silicon solar cells have efficiences up to 30%.

In an entirely different historical background, photography using dyes with silver halides grains was first discovered in 1873 by Vogel. The first observation of injecting electrons by a dye molecule into the conduction band a semiconductor substrate was reported in 1960's. Highly efficiency sensitization of titanium dioxide (TIO_2) by a Ruthenium dye was first published in 1991,[3] which led to the development of new a concept of generating electricity from sunlight.

This approach of generating electricity from has many advantages over the silicon solar cell technology. The DSSC are much cheaper to manufacture compared crystalline silicon solar cell. Though various other wide band gap semiconductors such as SnO_2, ZnO, were studied, TiO_2 is chosen as an optimum semiconductor for DSSC because it has many advantages, including long term thermal stability and photo-stability. Also It is cheap, abundant, non-toxic, biocompatible, and widely used in healthcare products and paints.

In 1988, Michael Gratzel and other researches discovered that TiO_2 is the best suited semiconductor for chemisorbing the dye for efficient light harvesting and energy conversion. Substantial improvements in efficiency have been achieved the record AM 1.5 efficiency for a DSSC is ca 10 %. [2,19]

A schematic diagram of DSSC is shown in figure 4, from left to right, the cells components are described as follows:

i) Transparent conducting SnO_2:F substrate

ii) Titanium dioxide film, photosensitizer dye (adsorbed as shown figure 4)

iii) Redox electrolyte (iodine and potassium iodide in acetonitrile solution) or regenerating the oxidized dye and,

iv) Conducting SnO_2:F with Pt as counter electrode

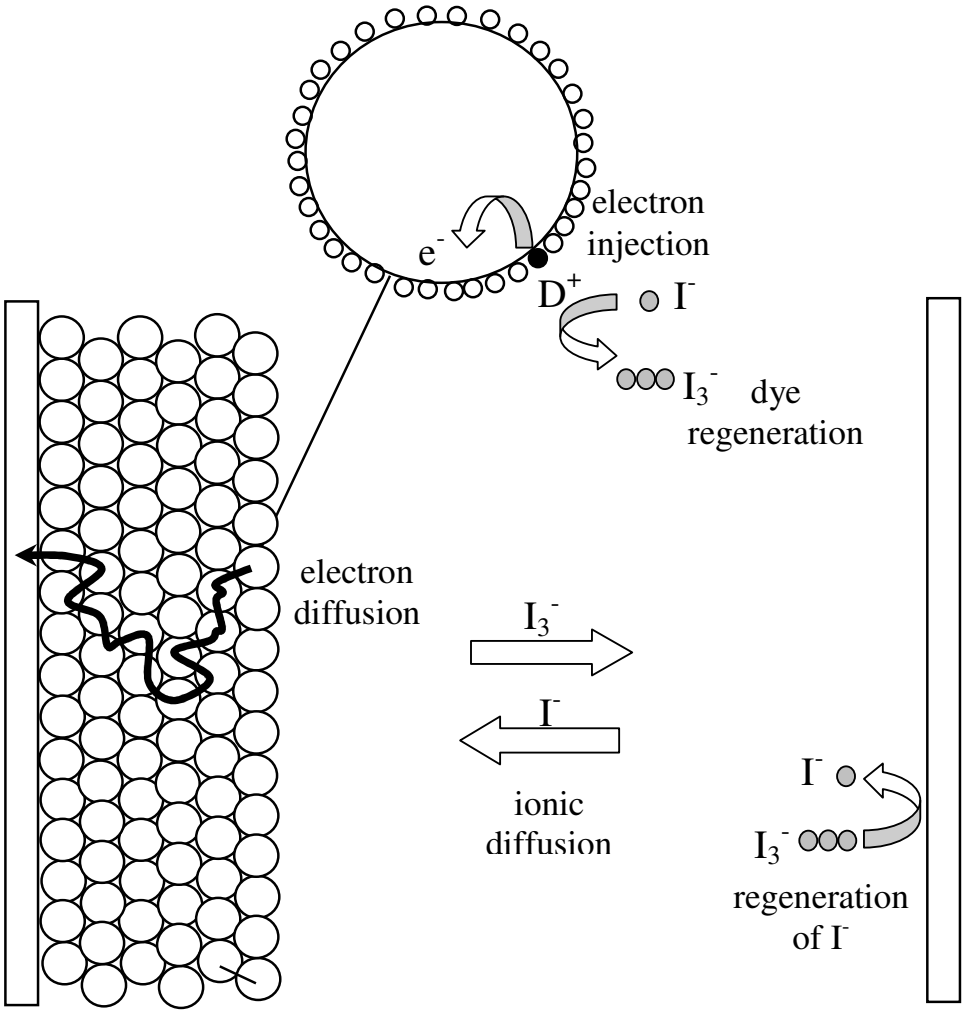

***Figure 4**. Schematic representation of the solar cell*[20]

The nanocrystalline TiO_2 films is generally prepared using:

Commercially available colloidal TIO_2 powder with particle size of 25-30 nm or a commercial product P25 (Degussa). As shown in the diagram of Figure2 when the light is illuminated on the devices, the dye attached to TiO_2 is photo-excited and injects an electron into of conduction band of TiO_2.

Due to the nanocrystalline, high porous and sponge- like nature of TiO_2 films, it is possible for the light to penetrate through the hundreds monolayers of adsorbed dye molecules. The electron transfer takes place via metal-to-ligand charge transfer (MLCT) transition.

Chelating groups such as carboxylic acids, which are grafted onto TiO_2 with strong electronic coupling between 3d orbitals of TiO_2 and P orbitals of bipyiridine ligand act as brinding units for efficient electron transfer. The dye behaves exactly as chlorophyll does in natural photosynthesis. In the DSSC, the dye absorbs the light and utilizes this energy to induce electron transfer. Photoinjected electrons percolate rapidly through the TIO_2 film and are quantitatively collected by the conducting SnO_2 glass. The dye is reduced back to its original state by the electrolyte. This regeneration of the dye by the electrolyte intercepts the recapture of the conduction band electron by the oxidized dye. The iodide is regenerated by reduction of triiodide at the counter electrode and the circuit is completed through the external load. Then the solar cell is regenerative.

The whole process of heterogeneous electron transfer and regeneration of the DSSC takes places as follows:

Anode: $S + h\nu \rightarrow S^*$ **Photo excitation**

$S^* \rightarrow S^+ + e^-(TiO_2)$ **Electron injection**

$2S^+ + 3I^- \rightarrow 2S + I_3^-$ **Regeneration**

Cathode: $I_3^- + 2e^-(Pt) \rightarrow 3I^-$

Cell: $e^-(Pt) + h\nu \rightarrow e^-(TiO_2)$

A Dye-sensitized solar cell is composed of four specific parts: the titanium oxide that is like the heart of the device, the dye where the incident light is absorbed, the electrolyte that holds the regeneration of the sensitizer and the counter-electrode.

1.2.3.1. The semiconductor – Titanium oxide

Titanium oxide exists in three different crystal structures: rutile, anatase and brookite. Anatase and rutile are the most common and they are both tetragonal phases (Fig. 5) with similar densities (anatase 3.89 g/cm^3 and rutile 4.26 g/cm^3). They are transparent in the visible and the near infrared ranges, and have band gaps of 3.0 eV (rutile) and 3.2 eV (anatase).

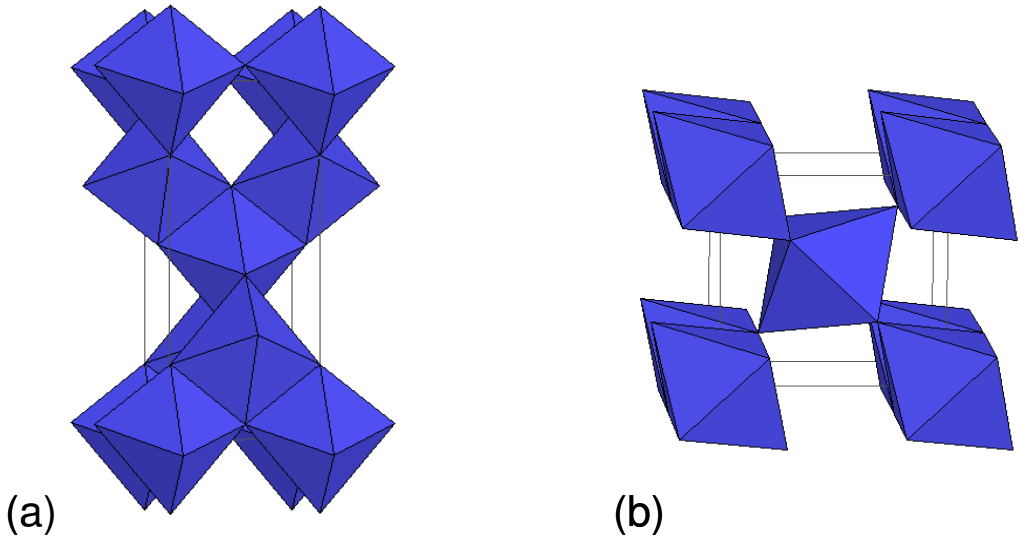

Figure 5. *The structure crystalline of TiO_2. a) Anatase, b) Rutile*

Rutile is thermodynamically more stable than anatase under normal conditions (1.2-2.8 kcal mol^{-1})[21,22] and its transformation to anatase in generally observed at temperatures above 700°C at atmospheric pressure.

Titanium oxide is very commonly used for industrial applications because its very interesting properties, such as high refractive index (paint

industry) and nontoxicity (cosmetics and health care products). Titanium oxide is also an attractive candidate for other industrial applications because it is hard and chemically resistant. Additionally, the thin film production of titanium oxide is of special interest for anti-reflection coatings,[23] dielectric materials, sensors.[24]

At the present time, titanium oxide is of great interest for photoelectrochemical applications. They include photocatalytic destruction of organic pollutants in wastewater,[25,26] and photogeneration of electricity using dye-sensitized solar cells.[3-13]

1.2.3.2 The Electrolyte

The electrolyte used in the DSSC consists of iodine (I^-) and triiodide (I_3^-) as a redox couple in a solvent with possibly other substances added to improve the properties of the electrolyte and the performance of the operating DSSC.

The I^- / I_3^- redox couple have listed the ideal characteristics of the redox couple for the DSSC electrolyte:

1. Redox potential thermodynamically (energetically) favorable with respect to the redox potential of the dye to maximize cell voltage;
2. High solubility in the solvent to ensure high concentration of charge carriers in the electrolyte;
3. High diffusion coefficients in the used solvent to enable efficient mass transport;
4. Absence of significant spectral characteristics in the visible region to prevent absorption of incident light by the electrolyte;
5. High stability of both the reduced and oxidized forms of the couple to enable long operating life;
6. Highly reversible couple to facilitate fast electron transfer kinetics;
7. Chemically inert toward all other components of the DSSC.

Since the discovery of the DSSC about seventeen years ago,[3] no redox couple preceding the performance of the I^-/I_3^- couple in the DSSC has been discovered.[27] The I^-/ I_3^- redox electrolyte is prepared by adding I_2 to the solvent together with some iodine salt such as KI ,[3] LiI.[28]

A report [27] clearly highlights the importance of the cation of the iodine salt to the performance of the DSSC. The photocurrent output was found to increase linearly with decreasing cation radius, the smallest cation Li^+ and K^+ showing the best performance.

The results also showed that the relative concentration of I^{3-} to I^- in the electrolyte is an important factor to the cell performance. The electrolyte used in the present work was: 0.1 M LiI, 0.6 M tetrabutylammonium iodide, 0.1 M I_2 and 0.5 M 4-tertbutylpyridine in acetonitrile

1.2.3.3. The Solvent

Stanley et al.[29] have given a number of criteria for a suitable solvent for a high efficiency liquid electrolyte DSSC:

1. The solvent must be liquid with low volatility at the operating temperatures (-40℃ - 80℃) to avoid freezing or expansion of the electrolyte, which would damage the cells;
2. It should have low viscosity to permit the rapid diffusion of charge carriers;
3. The intended redox couple should be soluble in the solvent;
4. It should have a high dielectric constant to facilitate dissolution of the redox couple;
5. The sensitizing dye should not desorb into the solvent;
6. It must be resistant to decomposition over long periods of time;
7. And finally from the point of view of commercial production, the solvent should be of low cost and low toxicity.

Examples of the solvents used in the electrolytes in DSSCs are: acetonitrile,[3] methoxyacetonitrile,[30] methoxypropionitrile,[31] glutaronitrile,[32] butyronitrile,[33] ethylene carbonate[3] and propylene carbonate.[34].

1.2.3.4. The dye – N 719

The dye is a very important component of a dye- sensitized solar cell, because it is there where the quantum conversion is performed.

The dye used in this work was bis(tetrabutylammonium) cis-bis(thiocyanato) bis (2, 2'- bipyridine- 4 - carboxylic,4'- carboxylate) ruthenium(II) which is known as N 729 (Figure 6). This dye is adsorbed on the surface of the nanostructured TiO_2 film by soaking the film in an ethanolic solution of N719. The bonding between the dye and the TiO_2 should give high stability, dense packing and efficient charge injection. The dye N719 is one of the most efficient and most studied dyes of nanostructured solar cells.

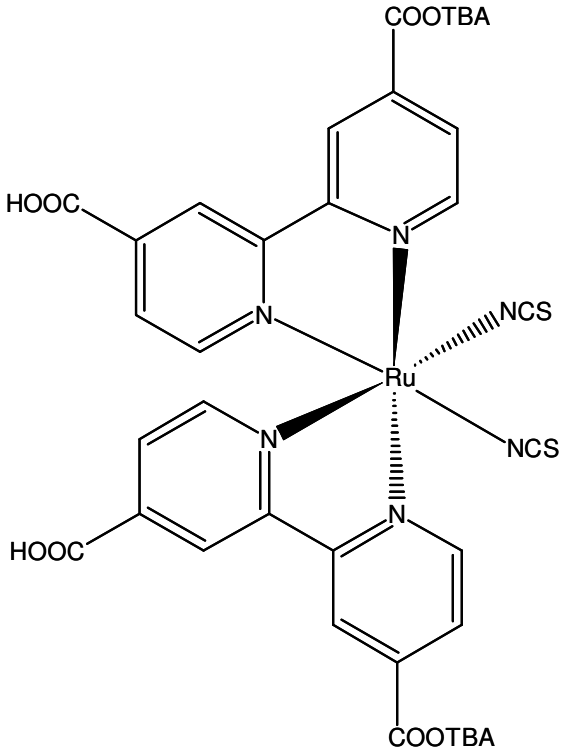

Figure 6. *Structure of the ruthenium dye employed as sensitizer of dye-sensitized solar cell (Dye 719).*

Infrared spectroscopy studies have suggested a bridging or bidentate chelate coordination (Figure 7) to the TiO_2 surface via two carboxylate groups per dye molecule.[35,36] The dye exists in two redox states in the solar cell (Ru^{2+} and Ru^{3+}). The valence level of neutral ruthenium (Ru4d) contains eight electrons (d^8) and therefore Ru^{2+} and Ru^{3+} have six and five d-electrons, respectively. The redox potential for the dye (Ru^{2+}/Ru^{3+}) dissolved in ethanol is 1.1 V versus Normal Hydrogen Electrode,[37]corresponding to the energy -5.6 eV versus vacuum. The highest occupied molecular orbitals are almost entirely of Ru and NCS character and the lowest unoccupied molecular orbitals are mainly of dicarboxybipyridine (dcbpy) ligand character.[38] The dye absorbs light between 300-800 nm. Two absorption maxima in the visible wavelength region, 400 nm and 550 nm (when adsorbed onto the TiO_2 film) are due to metal to ligand charge transfer (MLCT) transitions, in which an electron, localized mainly on the Ru-NCS center in the initial state, is transferred to the orbital set on the dcbpy ligands.[39] Additives such as 4-*tert*-butylpyridine (4TBP), 1-methylbenzimidazole (MBI) and carboxylic acids are usually added to the electrolyte in order to improve the performance. The bases, 4TBP and MBI, are rather bulky molecules.

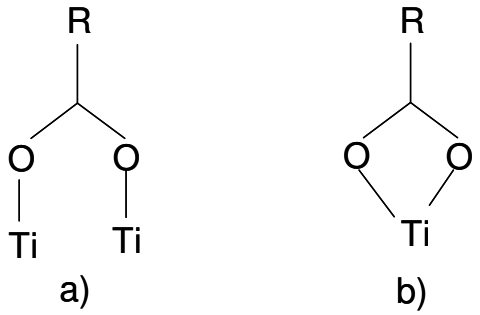

Figure 7. *Possible adsorption geometries of a carboxylate group (a) bridge and (b) bidentate chelate on a titanium dioxide surface.*

1.2.3.5. Recombination

Recombination of the generated electrons with holes in the dye-sensitized nanostructured TiO_2 electrode can in principle occur both after the electron injection or during its migration through the TiO_2 electrode on its way to the electrical back contact.

The illumination of the dye-sensitized electrode, initially in equilibrium, generates a transient electric field between the injected electrons in the TiO_2 and the oxidized species in the electrolyte. This electric field could in principle oppose further charge separation and promote recombination. However, in the dye cell the mobile ions in the electrolyte can easily rearrange and effectively hinder the light induced opposing fields, thus enabling an efficient charge separation.[40]

In the silicon solar cells the recombination of charge carriers in trap states at surfaces, grain boundaries, and in the bulk degrades the cell performance easily, and thus semiconductor materials of high crystal purity are required. In the dye-sensitized TiO_2 electrode, there is, on the contrary a vast amount of particle boundaries and a huge surface to volume ratio. Yet the dye solar cell does not seem to suffer from the recombination losses at the grain boundaries, at all.

The reason for this is that only electrons are transported through the semiconductor particles, while holes (oxidized ions) are carried by the electrolyte. The dye cell works as a majority carrier device, similar to a metal-semiconductor junction or a Schottky diode. In the absence of holes in the semiconductor particles, the recombination occurs mostly by loss of electrons to an oxidized dye molecule or to a hole in the electrolyte, i.e. the oxidized triiodide.

The former process is negligible, as assumed in most electrical models of the cell, but may be important in near open circuit conditions, i.e. in the case of the accumulation of electrons into the TiO_2 particles.[41] The latter recombination pathway, on the other hand, is made inefficient by reaction

kinetic reasons. The net recombination reaction at the TiO_2-electrolyte interface is a two electron reaction

$I_3^- + 2e^- \rightarrow 3I^-$ ……(a)

composed of sub-reactions

$I_3^- \leftrightarrow I_2 + I^-$ ……..(b)

$I_2 + e^- \rightarrow I_2^-$ …… (c)

$2I_2^- \xrightarrow{slow} I_3^- + I^-$ …….. .(d)

the last of which is a slow dismutation reaction and rate limiting in the net recombination reaction. Reaction equation (c) shows that the actual electron acceptor in the recombination reaction is I_2.

CHAPTER II

2. EXPERIMENTAL PROCESS

This chapter describes the preparation and the experimental techniques have been used for characterization of the electrodes and of the solar cells.

The electrodes of the solar cells was prepared by two ways :

- Method A. Mix metal salts of aluminum into the TiO_2 suspension
- Method B. Electrochemical process for insertion of aluminum ion into TiO_2 film.

2. 1. Electrode preparation. Method A.

Nanostructured TiO_2 films coated with aluminum oxide were prepared by the following method. Different amounts of $AlCl_3$ or $Al(NO_3)_3$ were added to the aqueous solution of TiO_2 powder (Degussa P25) in order to obtain between 0.1 and 3.6 wt.% of aluminum oxide in the resulting film. In addition, pure TiO_2 films were prepared as a reference. The suspensions were stirred with a magnetic stirrer for 2 min and agitated ultrasonically for 30 min.

The resulting suspension was applied onto a conducting glass substrate (SnO_2:F- coated glass, resistance 8 Ω/square) by doctor blading, using adhesive tape as frame and spacer. After deposition, the water was allowed to evaporate at room temperature for 2 h.

The dry powder film was put between two planar steel press plates and a pressure of 600 kg cm^{-2} was applied using a hydraulic press.[6,7] The working electrode was annealed in air at 530 ℃ for 30 min. The mean thickness of the obtained films was around 18 to 20 μm, as measured by profilometry (Dektak 3, Veeco Instruments).

2.2 Electrode preparation. Method B.

TiO_2 electrodes were prepared as explain before (Method A) without aluminum salt. In addition, Al_2O_3 films were prepared in a similar way using Degussa Alumiumoxid C powder.

Electrodes were characterized using Raman and UV-vis (Ocean Optics HR2000 with integrating sphere) spectroscopies. Furthermore, the Al-content in the films was determined using neutron activation analysis.

2.3 Solar Cell Preparation

The electrodes were dye-sensitized by submerging the substrate with the deposited film for 12 h in a dye-bath consisting of 0.5 mM cis-bis(isothiocyanato)-bis(2,2´bypiridyl-4,4´dicarboxylato) ruthenium (II) bis-tetrabutylammonium (N719) dye in ethanol. The excess of dye was removed by rinsing the surface of the electrode with ethanol.

The counter electrode was platinized by applying a drop of 5 mM of dry H_2PtCl_6 in isopropanol onto a conducting glass substrate and annealing it in air at 380℃ for 10 min. The solar cell was prepared by the fabrication of a 1.5 cm^2 sandwich DSSC. To fill the cell with the electrolyte a hole was made in the counter electrode plate.

The cell was assembled using Surlyn (Dupont), which is a thin plastic sheet (60μm) that melts at around 120℃. After assembly, the cell was filled with the electrolyte (0.1 M LiI, 0.6 M tetrabutylammonium iodide, 0.1 M I_2 and 0.5 M 4-tertbutylpyridine in acetonitrile). Thereafter, the hole was sealed with surlyn and a cover glass.

Silver paint was put on the electrodes to assure the electrical contact with the external circuit. All used chemicals were of reagent grade and purchased from Aldrich (See *Scheme 2*).

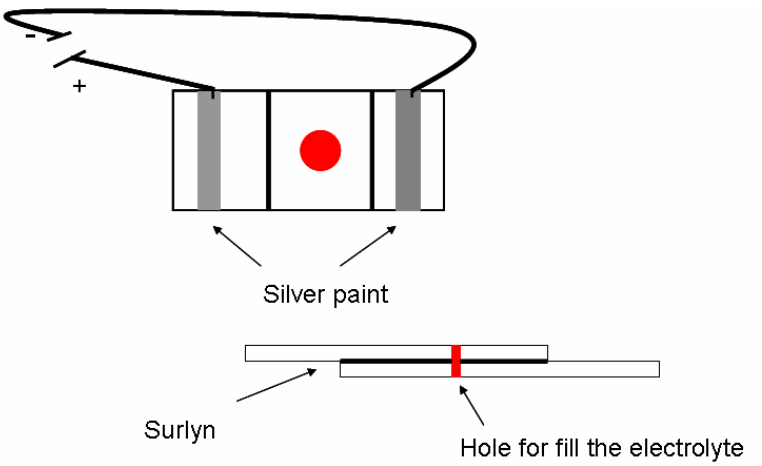

Scheme 2. *Schematic representation of a solar cell.*

2.4 Experimental Techniques.

In this work have been used the following techniques for characterized the electrodes and the solar cells:

2.4.1. Photoelectron spectroscopy.

The technique of photoelectron spectroscopy (PES) measures the ionization energies of molecules when electrons are ejected from different orbitals, and uses the information to infer the orbital energies.

As the energy is conserved when a photon ionizes a sample, the energy of the incident photon hν must be equal to the sum of the energy of ionization, I, of the sample and the kinetic energy of the photoelectron, the ejected electron (see Figure 8):

$$h\nu = \frac{1}{2} m_e V^2 + I \quad \text{.....(4)}$$

This equation can be refined in two ways; the photoelectrons may originate from one of a number of different orbitals, each one having a different ionization energy. Hence, a series of different kinetic energies of the photoelectrons will be obtained, each one satisfying:

$$h\nu = \frac{1}{2} m_e V^2 + I_i \text{ .....(5)}$$

where I_i is the ionization energy for ejection of an electron an orbital i. Therefore, by measuring the kinetic energies of the electrons, and knowing ν, these ionization energies can be determined.

Photoelectron spectra are interpreted in terms of an approximation called Koopma's theorem, which states that the ionization energy I_i is equal to the orbital energy of the eject electron ($I_i = -\varepsilon_i$). Then it is possible to identify the ionization energy with the energy of the orbital from which it is ejected.

In XPS, the energy incident photon is so great that electrons are ejected from the inner cores. As a first approximation, core ionization energy are insensitive to the bonds between atoms because they are too tightly bound to be greatly affected by the changes that accompany bond formation, so core ionization energies are characteristic of the individual atom rather than of the overall molecule. Consequently XPS, gives lines characteristic of the elements present in a compound.[42]

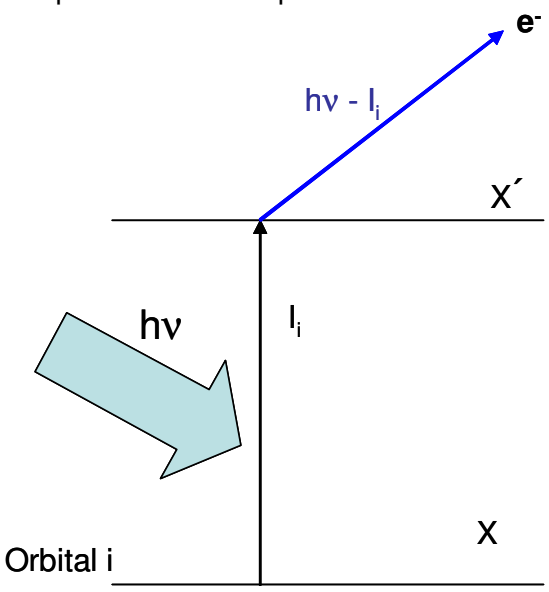

***Figure 8**. An incoming photon carries an energy hν an energy I_i is need to remove an electron from an orbital i, and the difference appears as the kinetic energy of the electron.[42]*

The photoelectron spectroscopy (PES) measurements were performed in an ESCA 300 spectrometer, using monochromatic Al Kα radiation (1486.7eV). The electron take off angle was 90°. The insulating Al_2O_3 was measured using a flood gun and energy calibrated using the Al2p signal. PES measurements, as well as X-ray absorption spectroscopy (XAS) measurements, were also performed using a Scienta SES-200 hemispherical electron analyzer and synchrotron radiation at BL I411 at the Swedish national laboratory MAX-lab in Lund. The take off angle used was 70°, and the angle between the photon polarization and photoelectron direction was 0°.

The PES spectra were energy calibrated by setting the Ti2p substrate signal to 458.56eV and the Ti2p XAS spectra were energy calibrated through measurement of the Ti3p peak using first and second order light.

The intensity in a PES measurement depends on the surface density of the elements, the cross section for ejection of photoelectrons, the mean free path of the electrons in the sample, and on the transmission of the spectrometer. The mean free path of the electrons depends, in turn, on their kinetic energy. Thus by changing the photon energy, the surface sensitivity in a PES measurement can be controlled. In the present investigation, measurements using lower photon energies are more surface-sensitive than those performed using higher photon energies.

In the measurements comparing intensity of the Ti3p signal with the Al2p signal for different photon energies the transmission of the spectrometer is expected to be very similar. XAS and PES was performed on an Al-modified TiO_2 electrode containing 11.8 wt% Al, where as the high concentration of Al is expected to give most clear result. Pure TiO_2 and the Al_2O_3 samples were used as reference.

2.4.2. Scanning Electron Microscopy

In this technique a focused beam of electrons with a well defined de Broglie wavelength replaces the lamp found in traditional light microscope. Instead of glass or quartz lenses, magnetic fields are used to focus the beam. Electrons scattered from a small irradiated area are detected and the signal is sent to a video screen. An image of the surface is then obtained by scanning the electron beam and the detector across the sample.

The electrons from a thermionic or field – emission cathode are accelerated by a voltage of 1-50 kV between cathode and anode. Then the beam is condensed and collimated by pole- pieces (magnetics lens) until it dissipates its energy in the sample. The emitted electrons consist of secondary electrons (SE), backscattered electrons (BSE), and Auger electrons. Both SE and BSE carry information about the sample topography.[22]

Surface morphologies were studied by Scanning electron Microscopy using a LEO 1530. The samples were prepared on a substrate of conductor glass, a few amount of silver paint was used for maintain the electrical contact.

2.4.3. Raman spectroscopy

In this spectroscopy, molecular energy levels are explored by examining the frequencies present in the radiation scattered by molecules. These scattered photons constitute the lower-frequency Stockes radiation from the sample. Other incidents photons may be collected by the molecules, and emerge as higher frequency anti Stockes radiation**.** The component of the radiation scattered in the forward direction, without change in frequency, is called Rayleigh radiation.

Lasers are used as the radiation sources in Raman spectrometers for two reasons:

First, the shifts in frequency of the scattered radiation with respect to the incident radiation are quite small, so highly monochromatic radiation form a laser is required if the shifts are to be observed.

Second, the intensity of the scattered light is low, so intense incident beam, such as those from lasers are need.[42]

Raman spectrometry studies in the present work were carried out using a Renishaw Ramanscope with He/Ne laser, (633 nm, 20 mW). The samples have been measured directly. A schematic representation is shown in the Figure 9.

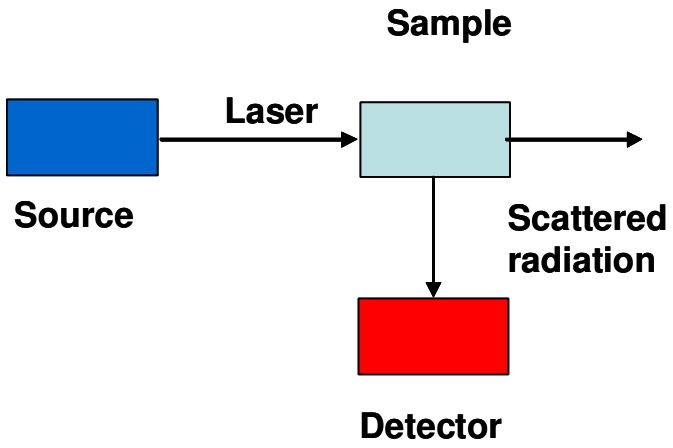

Figure 9. *The basic set-up of a Raman spectrometer is shown. The detector is orthogonal to the direction of incident radiation, so as to observe only the scattered light.*

2.4.4. Nuclear Activation Analysis

In typical NAA, stable nuclides (^{A}Z, the target nucleus) in the sample undergo neutron capture reactions when exposed to flux of (incident) neutrons. The radioactive nuclides (^{A+1}Z, the compound nucleus) produced in this activation process will, in most cases, decay through the emission of a beta particle (β) and gamma ray(s) with a unique half-life. A high-resolution

gamma-ray spectrometer is used to detect these "delayed" gamma rays from the artificially induced radioactivity in the sample for both qualitative and quantitative analysis.

The energies of the delayed gamma rays are used to determine which elements are present in the sample, and the number of gamma rays of a specific energy is used to determine the amount of the element in the sample.

The measured count rate (R) of the gamma rays from the decay of a specific isotope in the irradiated sample can be related to the amount (n) of the original, stable isotope in the sample through the following equation:

$$R = \varepsilon I_\gamma \quad A = \varepsilon I_\gamma n \varphi \sigma (1-e^{-\lambda t_i}) e^{-\lambda t_d} \ldots\ldots\ldots\ldots\ldots\ldots (6)$$

where:

R = measured gamma-ray count rate (counts per second)
A = absolute activity of isotope ^{A+1}Z in sample
ε = absolute detector efficiency
I_γ = absolute gamma-ray abundance
n = number of atoms of isotope ^{A}Z in sample
φ = neutron flux (neutrons·cm^{-2}·sec^{-1})
σ = neutron capture cross section (cm^2) for isotope ^{A}Z
λ = radioactive decay constant (s^{-1}) for isotope ^{A+1}Z
t_i = irradiation time (s)
t_d = decay time (s)

The neutron flux φ, neutron capture cross section σ, absolute detector efficiency ε, and absolute gamma-ray abundance I_γ are known, thus the number of atoms n of isotope ^{A}Z in the sample can be calculated directly. In most cases, however, a standard is irradiated and counted under similar conditions as the sample, and the mass of the element in the sample (W_{sam}) is found by comparing the measured count rates (R) for the sample and standard through the following equation:

$$W_{sam} = W_{std} \frac{R_{sam}}{R_{std}} \quad \ldots\ldots\ldots\ldots \quad (7)$$

where:

W_{sam} = mass of element in sample (g)
W_{std} = mass of element in standard (g)
R_{sam} = gamma-ray count rate from the sample (counts per second)
R_{std} = gamma-ray count rate from the standard (counts per second)

The amount of aluminum in the samples was determined using k_0 based neutron activation analysis.[43]The scratched film were weighed (50 mg or 70 mg) and put in polyethylene bags; 500 μg of sodium pellet of 15 mm diameter and 2 mm height was used as standard. These samples were put together inside polyethylene capsules. The irradiations were carried out for 10 min in the RP-10 reactor of the Instituto Peruano de Energia Nuclear at a neutron flux of $0.5x10^{12}$ ncm^2 s^{-1} using a pneumatic system. After adequate decay times, the induced radioactivity of the samples and sodium standard was measured by high resolution gamma-spectrometry using a HP Ge detector, and a source-detector distance of 160 mm.[44]

The detector resolution was 1.9 keV for the 1408 keV ^{152}Eu peak. The spectra were acquired with a Canberra GC multichannel analyzer and transferred to a personal computer. The evaluation of gamma spectra was made using the DB Gamma V5.0 software. Elemental concentrations were determined by the k_0 method, using the Högdahl convention.[45] The Al wt. % measured for films obtained with different amounts of $Al(NO_3)_3$ and aluminum ions added to TiO_2 suspension are shown in Table 1 and Table 2. A good correlation is observed between the amount of aluminum added and measured in the analyzed.

2.4.5. Cyclic Voltammetry.

Cyclic voltammetry involves the imposition of different waveform as the potential on the working electrode; and the simultaneous measurement of the current. The potential is normally generated with a function generator, and

applied to the cell through a potentiostat. The current –potential curves can be displayed with X-Y recorder at slow scan rates.

Negative and positive turn- round potentials E_t^c and E_t^a are usually chosen in aqueous or non-aqueous media. By scanning the potential between these limits, it is possible to obtain highly reproducible current- voltage behaviour. In general the reproducible behaviour depends on a series of parameters, including electrolyte purity, and choice of turn-round potential and rate of change of potential. The Figure 10 has shown an electrochemical system.

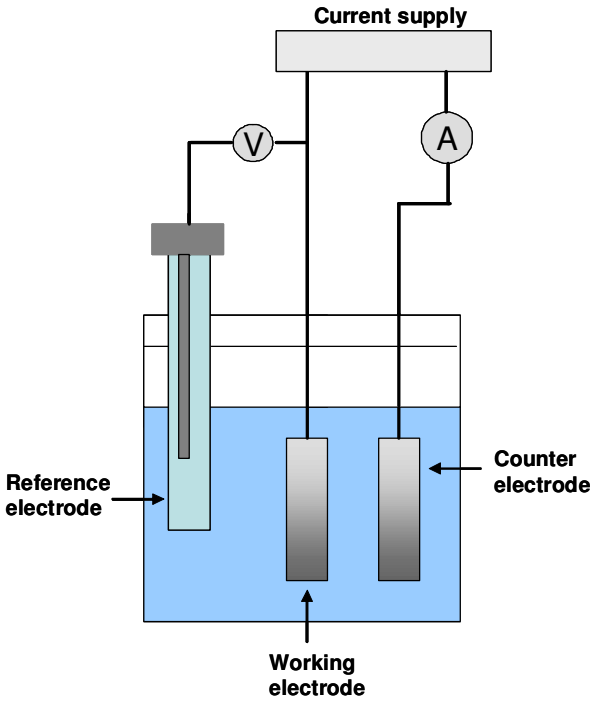

***Figure 10**. Electrochemical system*

2.4.6. Chronoamperometry.-

The potential is stepped in a square wave shape to a potential just above the position where the peak would appear in linear sweep voltammetry. The current is then monitored as function of time (Figure 11).

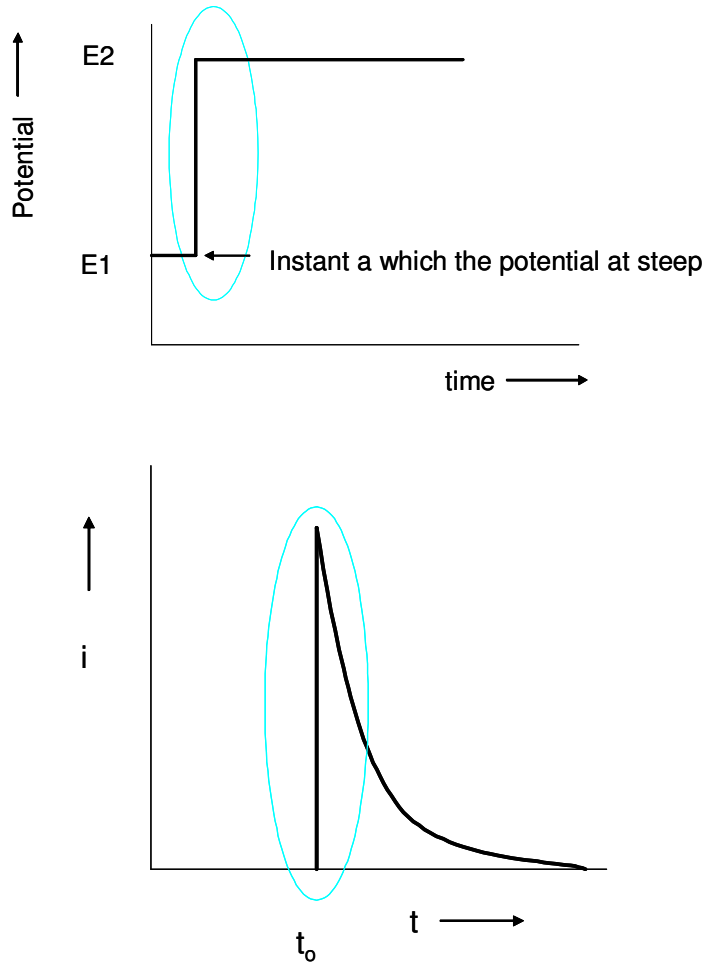

Figure 11. *Schematic representation of the chronoamperometry*

The TiO_2 electrodes were electrochemically modified with aluminum as follows: the TiO_2 electrode served as the working electrode in a standard 3-electrode system, with a coiled Pt wire counter electrode, and an Ag/AgCl/ saturated LiCl in polypropylene carbonate reference electrode, all connected

to an ECO Chemie Autolab PGStat 10 electrochemical interface. Aluminum perchlorate nonahydrate and polypropylene carbonate (Aldrich) was used to prepare a 1.0M $Al(ClO_4)_3$ electrolyte solution, which was partially dried over 3Å molecular sieves.

The final water content of the electrolyte was estimated to be a few percent. The electrolyte was purged with nitrogen and a nitrogen atmosphere was maintained during the experiments. Chronoamperometric methods were used to insert controlled amounts of aluminum: the potential was stepped to -1.3 V for different periods of time. Electrodes were annealed at 400℃ for 10 min afterwards to remove adsorbed perchlorate ions and adsorbed organic material.

2.5 Solar cell characterization

2.5.1 Incident Photon –to- Current Efficiency (IPCE)

The Incident Photon –to- Current Efficiency (IPCE) of a solar cell represents the ratio of the current of photogenerated electrons to the photon flux incident on the system. For the known photodiode family, the IPCE is named internal quantum efficiency $\eta(\lambda)$.[22]

$$\eta(\lambda) = \frac{j_{ph} / q}{P_{in} / hc} \quad \text{.....(8)}$$

where j_{ph} is the photocurrent density, P_{in} / hc is the photon flux for a given wavelength and q is the elementary charge.

Experimentally, the photocurrent is recorded during illumination with monochromatic light. Measuring the photoresponse and illumination intensity the IPCE can be calculated according to:[4,22]

$$IPCE = \frac{No \cdot of \cdot electrons \cdot generating \cdot the \cdot photocurrent}{Incident \cdot photons} = \frac{1240.j_{ph}}{\lambda(nm).P_{in}} \quad .....(9)$$

where λ is the wavelength in nanometer. The phocurrent results from a number of sequential events: absorption, electron injection, recombination and transport.

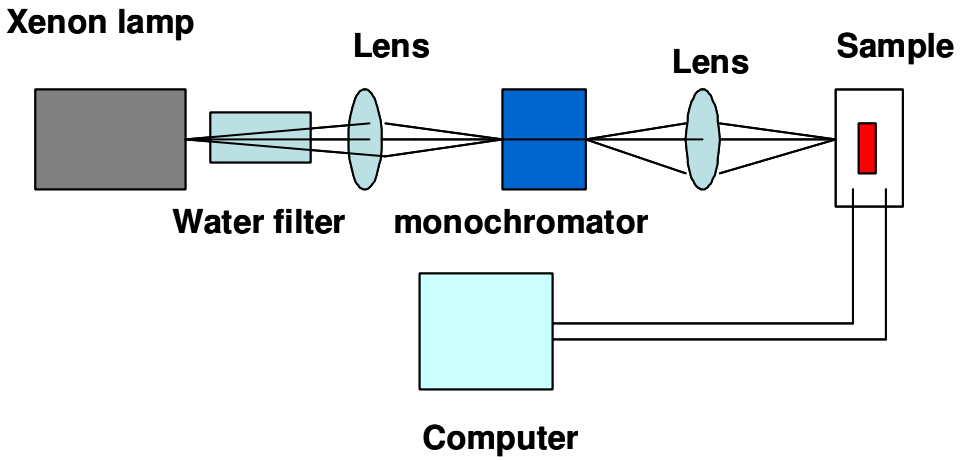

Figure 12. *Schematic of the experimental set-up for IPCE measurement for the solar cells*

The Incident photon-to-current conversion efficiency (IPCE) was recorded using a computerized set-up consisting of a xenon arc lamp (300 W Cermax, ILC Technology), a 1/8 m monochromator (CVI Digikröm CM 110), a Keithley 2400 source/meter, and a Newport 1830-C power meter with 818-UV detector head. The current-voltage (I-V) characteristics of the solar cells were recorded under simulated sunlight (Lightdrive 1000 from Fusion Lightning) using a computerized Keithley 2400 source/meter. The intensity was adjusted to match that of 1000 W m^{-2} with AM 1.5G spectral distributions using a filtered silicon diode (type BPW21R).

2.5.2 Intensity Modulated Photocurrent Spectroscopy (IMPS)

In Intensity Modulated Photocurrent Spectroscopy (IMPS) a small sinusoidal perturbation is superimposed onto a large dc illumination level. The time dependence incident illumination is:

$$I(t) = Io(1 + \delta.Sin(\omega t)) \quad \text{.....(10)}$$

where δ is the depth of the modulation and Io is the mean intensity. The phase and amplitude of the resulting ac photocurrent is measured as a function of the modulation frequency.

In a nanostructured semiconductor electrode the IMPS response reflects the electron transport through the nanocrystalline film to the back contact, under assumption that the electron life time is much larger than the required transport time. The time constant associated with the charge transport can be calculated from the angular frequency at which the maximum (90^o) photocurrent phases shifted occurs:

$$\tau = \frac{1}{\omega_{\max}} \quad \text{.....(11)}$$

For nanocrystalline systems it has been shown that $\omega_{\max}$ depends on the light intensity.

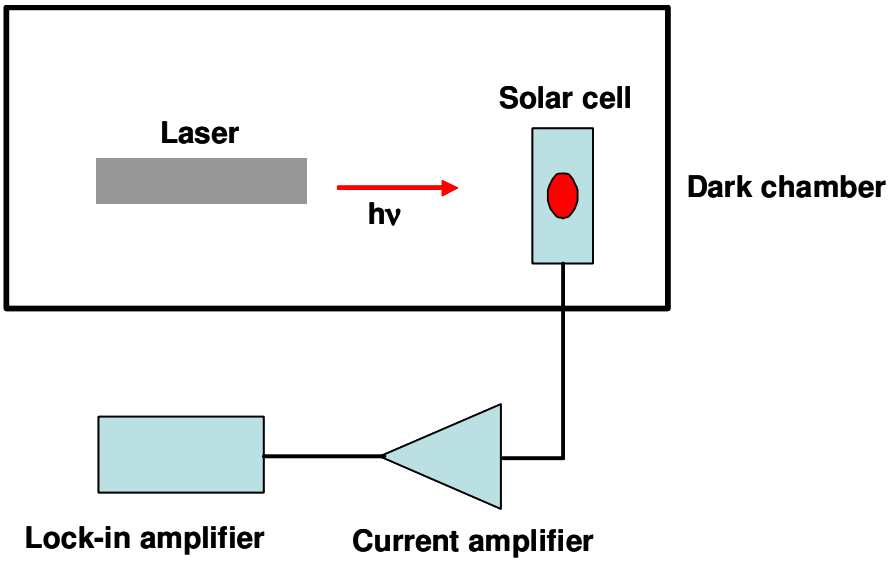

Figure 13. *Experimental arrangement for intensity modulated photocurrent spectroscopy (IMPS)*

The electron concentrations, lifetimes and transport times in the dye-sensitized TiO_2 solar cells were measured in a system using a red light emitting diode (Luxeon Star 1W, λ_{max} = 640 nm) as the light source. Voltage or current traces were recorded using a 16-bit resolution data acquisition board (National Instruments PCI-6052E) in combination with a current amplifier (Stanford Research Systems SR570) and a custom-made system using electromagnetic relay switches. The relationship between potential and charge was investigated using a combined voltage decay / charge extraction method as follows:[46,47]

The solar cell was illuminated for 5 s under open circuit conditions and the voltage was left to decay for a certain period in the dark to a voltage *V*. Then the cell was short-circuited and the current was measured and integrated over 10 s to obtain $Q_{OC}(V)$. The charge accumulated in the TiO_2 film under short circuit conditions, Q_{SC}, was determined from the photocurrent decay transient upon switching off the light source (current integration time 10s).

Electron lifetimes and transport times were determined by monitoring the transient photovoltage (at open circuit) and, photocurrent response (at short circuit), respectively, after a small change in light intensity. To the base light intensity a small square wave modulation (<10 % intensity, 0.5 Hz) was added, and the step response was recorded.

The current and voltage responses were well fitted using first order decay kinetics and time constants were obtained accordingly. The direction of illumination was always from the TiO_2 electrode side. Special care was taken not to expose the solar cells to high light intensities for long times, in order to prevent significant intercalation of Li^+ ions, which affects the results.[18]

CHAPTER III

3. RESULTS.

This chapter describes the results have been obtained for the films and for the solar cells.

3. 1. Results. Method A.

Homogenous aqueous mixture of TiO_2 powder and different amounts of aluminum chloride or aluminum nitrate were prepared, these mixtures were spread out, allowed to dry, compressed, and finally annealed to oxidize the aluminum salt.

The aluminum oxide wt. % in the mixture was calculated by assuming that the aluminum salt completely oxidizes during annealing.

For example, 12g of TiO_2 was mixed with 0.05g of $Al(NO_3)_3$ and 18g of water (Milli-Q) at room temperature giving a mixture of 0.1wt. % aluminum oxide with respect to TiO_2.

The thickness of the aluminum oxide coating is estimated as follows: for the 0.1wt. % aluminum oxide mixture, 0.05g $Al(NO_3)_3$ gives 0.12g aluminum oxide. Using the density of Al_2O_3 (3.97g/cm^3), the volume of Al_2O_3 is calculated to be $3x10^{-8}m^3$. As the BET average surface area of P25 (TiO_2) is 55 m^2/g, the average thickness of the aluminum oxide layer is therefore estimated to be 0.05nm. The calculated thickness for different sample preparations is shown in Table 1.

wt. % Aluminum oxide Added	Thickness (nm)	Al wt. % added	Al wt. % measured
0.1	0.05	0.052	0.061
0.6	0.30	0.312	0.380
3.6	1.80	1.872	1.253
0.0	0.00	0.000	0.000

Table 1. *Calculated thickness for different amounts of added aluminum oxide. Comparison of the Al wt. % added using $Al(NO_3)_3$ and measured by neutron activation analysis. The aluminum oxide wt. % added was calculated if the salt was completely oxidized.*

Figure 14 shows a SEM image of a compressed aluminum oxide coated TiO_2 film (3.6 wt. % aluminum oxide) on SnO_2:F coated glass. In comparison with an uncoated TiO_2 film (not shown) we observe no specific differences indicating that the morphology remains unperturbed upon aluminum oxide coating. Similar SEM pictures were obtained for the other aluminum oxide concentrations (0.1% and 0.6%).

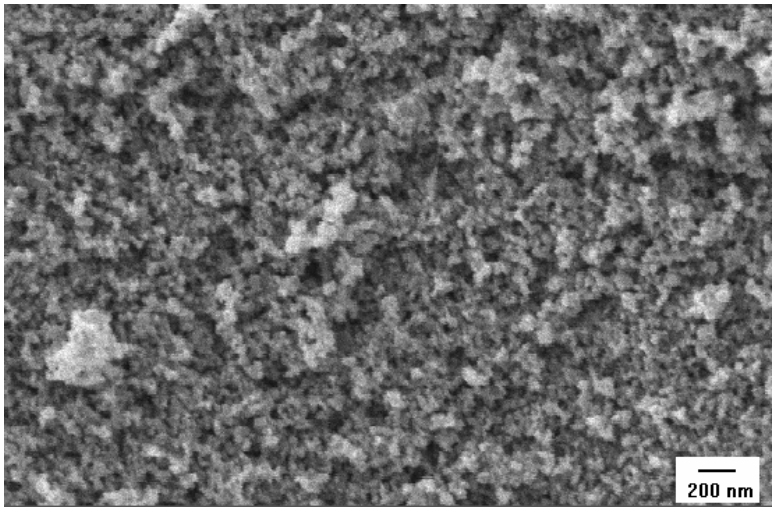

Figure 14. *SEM micrograph of a compressed aluminum oxide (wt 3.6%) modified TiO_2 film.*

Figure 15a shows the IPCE as a function of illumination wavelength for cells obtained using different amounts of $Al(NO_3)_3$ added to the TiO_2 suspension. It is observed that the film obtained with 0.1 wt. % of aluminum oxide shows a maximum IPCE of 0.80 at 550 nm.

Higher amounts of aluminum oxide in the film decreased the photoresponse. The film prepared with 0.6 wt. % of aluminum oxide has an IPCE of 0.75 at 550nm, whereas the film with 3.6 wt. % of aluminum oxide has an IPCE of only 0.35 at the same wavelength. The film with 0.1 wt. % of

aluminum oxide also has a relatively higher photoresponse for wavelengths longer than 600 nm.

The dye incorporation was measured by desorbing the dye from films into of 3mL of a 1mM KOH water solution and measuring the optical absorption spectra. The results of this experiments confirmed that the amount of aluminum oxide does not affect the amount of adsorbed dye significantly. To study the effect of the anion, $AlCl_3$ replaced the $Al(NO_3)_3$ salt and was added to the TiO_2 suspension. The corresponding IPCE spectra are shown in Figure 15b. Both aluminum salts have a similar behavior in the IPCE values, and the cells with the highest photoresponse are those obtained with 0.1 wt. % aluminum oxide. The cells obtained using aluminum nitrate has a higher photoresponse than the ones prepared using aluminum chloride.

Figure 15c compares the photoresponse for cells using TiO_2 and for the optimum cells (0.1 wt. % aluminum oxide) obtained upon adding $Al(NO_3)_3$ or $AlCl_3$ to TiO_2. It is clearly observed that the measured IPCE values increase with the aluminum oxide treatment. The maximum photoresponse of the cell was obtained when aluminum nitrate was used.

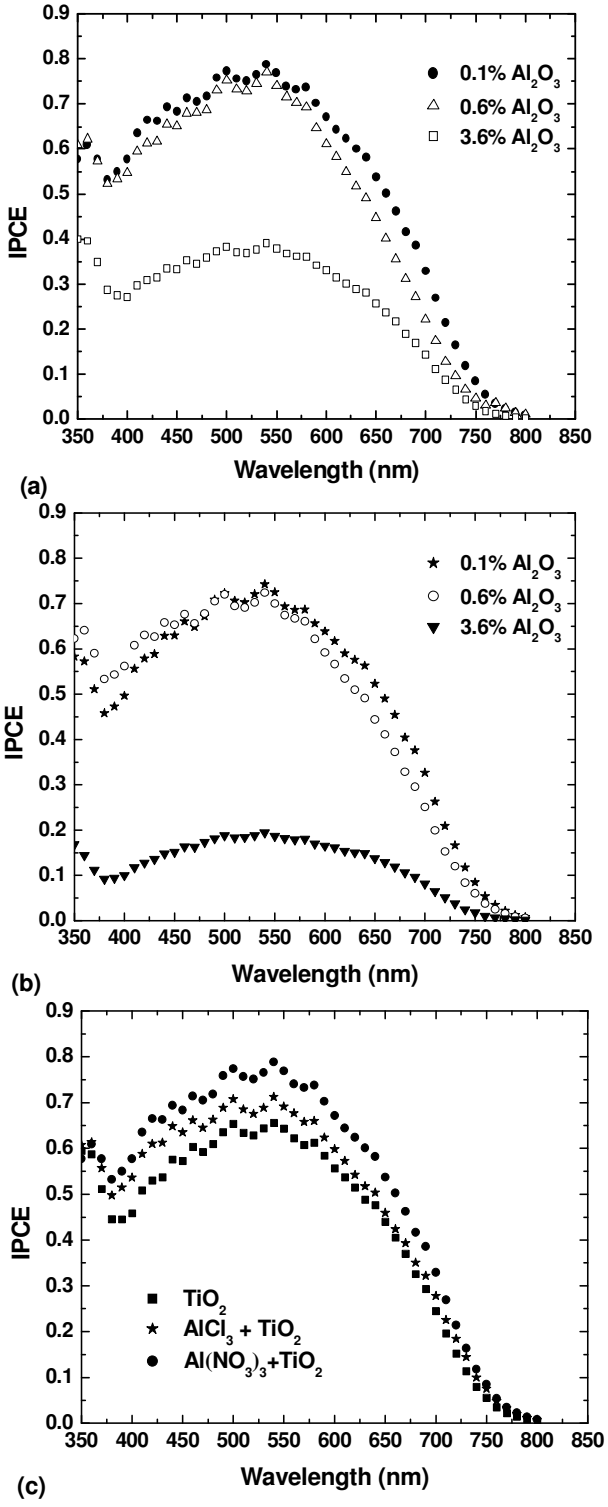

Figure 15. *(a) IPCE spectra for samples prepared by adding different amounts of $Al(NO_3)_3$ to the TiO_2 suspension. (b) IPCE spectra for samples prepared by adding different amounts of $AlCl_3$ to the TiO_2 suspension. (c) IPCE spectra for the solar cells prepared adding aluminum salts to TiO_2 suspension (0.1 wt. % aluminum oxide).*

The current-voltage curves for dye sensitized solar cell based on TiO_2 with and without the incorporation of 0.1 wt. % aluminum oxide using $AlCl_3$ or $Al(NO_3)_3$ are shown in Figure 16. The solar cell prepared by adding aluminum nitrate to the TiO_2 suspension (0.1 wt. % aluminum oxide) has the best improvement in the device performance under solar illumination.

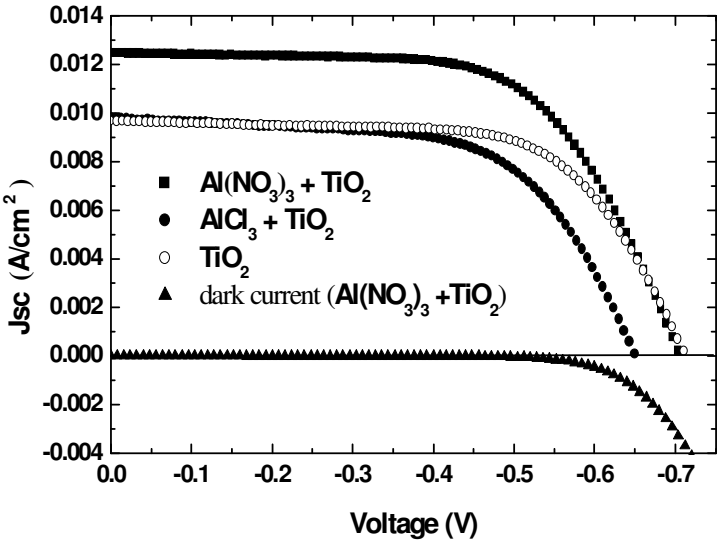

Figure 16. *Current-voltage curves of solar cells obtained using pure TiO_2 and adding $Al(NO_3)_3$ or $AlCl_3$ to TiO_2 suspension (0.1 wt. % aluminum oxide). The dark current of the $Al(NO_3)_3$ treated TiO_2 film is also shown. The light intensity during the experiments was 1000 Wm^{-2}.*

Figure 17 shows the short circuit current, I_{sc}, open circuit voltage, V_{oc}, fill factor, *FF*, and overall efficiency, η, for solar cells with different amount of aluminum oxide, obtained by adding $AlCl_3$ or $Al(NO_3)_3$ to the TiO_2 suspension. The efficiency and the short circuit current show similar trends, i.e. an increase for the cell with a concentration of 0.1 wt. % aluminum oxide and a decrease for the cells with concentrations of 0.6 wt.% and 3.6 wt. % aluminum oxide (Figure 17a).

On the other hand, the fill factor and open circuit voltage are relatively constant for all concentrations of aluminum oxide. The I_{sc} has a maximum

value for the cell prepared with 0.1 wt. % of aluminum oxide added to TiO_2. For cells with higher amount of aluminum oxide the I_{sc} decreased (Figure 17b). The open circuit voltage, V_{oc}, as well as the fill factor, *FF*, does not develop a significant change in the films. The V_{oc} changes between -0.6 and -0.73 V, whereas the *FF* changes between 0.56 and 0.63 (Figure 17c, 17d). The efficiency for solar cells of TiO_2 with 0.1 wt. % aluminum oxide obtained adding $AlCl_3$ and $Al(NO_3)_3$ and standard TiO_2 is 4.5, 5.6 and 3.9 %, respectively.

Figure 18a shows the extracted charge as function of voltage. The solar cell that has 0.1 wt. % aluminum oxide shows a larger amount of charge at any given voltage compared to the other cells. For this concentration and at a potential of -0.47 V, the charge is around 100 μCcm^{-2} (the area corresponds to the projected electrode area), which corresponds to a concentration of about 6 electrons per particle. For this calculation, it is assumed that the nanoparticles are spherical with a diameter of 25 nm, and that the porosity in the films is 57 %,[7] so that the number of TiO_2 particles in the film calculate to be $10^{14}cm^{-2}$.

When the charge extraction data is combined with the time delay, the lifetime of the electron (τ_e) can be calculated as follows:[47]

$$\tau_e = Q(t)\left(\frac{dQ(t)}{dt}\right)^{-1} \qquad (12)$$

This equation assumes a (pseudo) first order recombination reaction for the electrons. As the voltage decay takes place in the dark, the resulting lifetime is that of electrons in the dark, which may be longer than that under illumination. Figure 18b shows the lifetime of the electrons as a function of the potential of the dye-sensitized solar cell. The lifetime is in general quite long (>0.7 s). Aluminum oxide coverage results in longer electron lifetimes at potentials between -0.4 and -0.55 V.

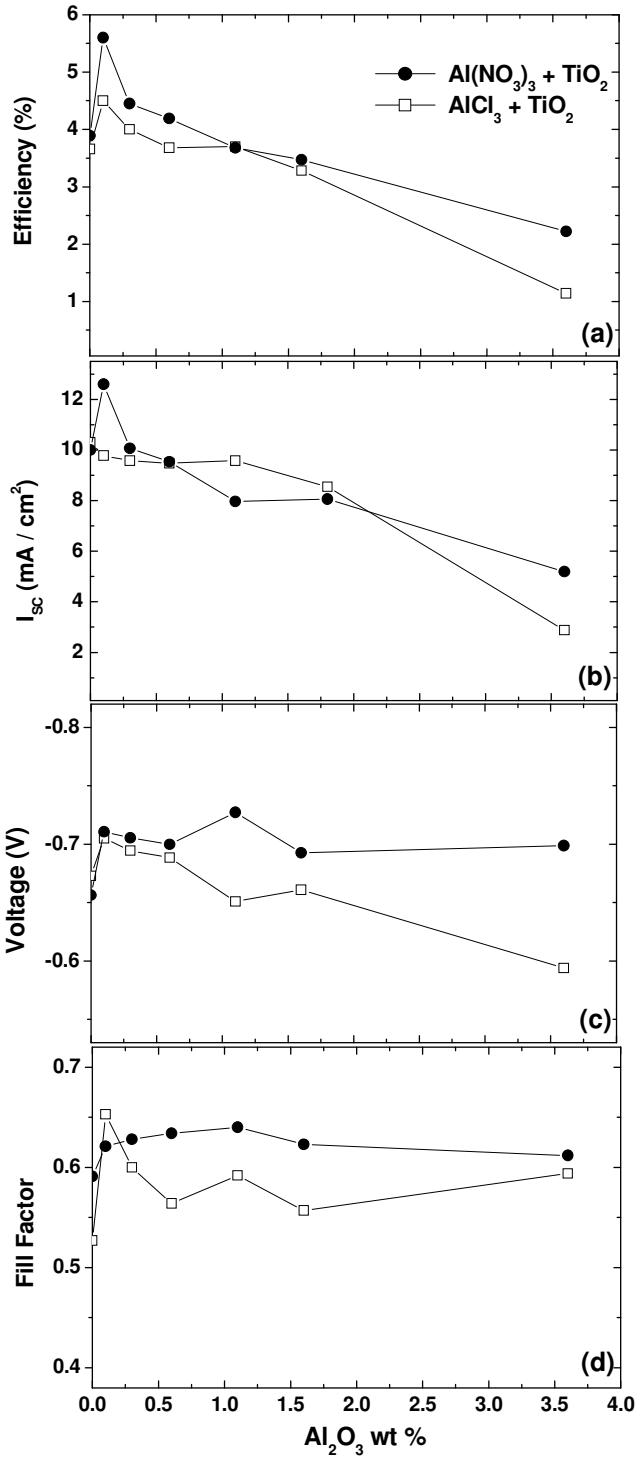

Figure 17. *(a) Efficiency, (b) short circuit current, (c) open circuit voltage and (d) fill factor for solar cells prepared with different amounts of $Al(NO_3)_3$ (•) or $AlCl_3$ ( ) to TiO_2. The light intensity during the experiments was 1000 W m^{-2}.*

Electron transport in the aluminum oxide modified TiO_2 solar cells was studied using intensity-modulated photocurrent spectroscopy (IMPS). The time constants (τ_{IMPS}) that are found are interpreted as transport times, which is a reasonable approximation if the transport time is much smaller than the electron lifetime.[48]

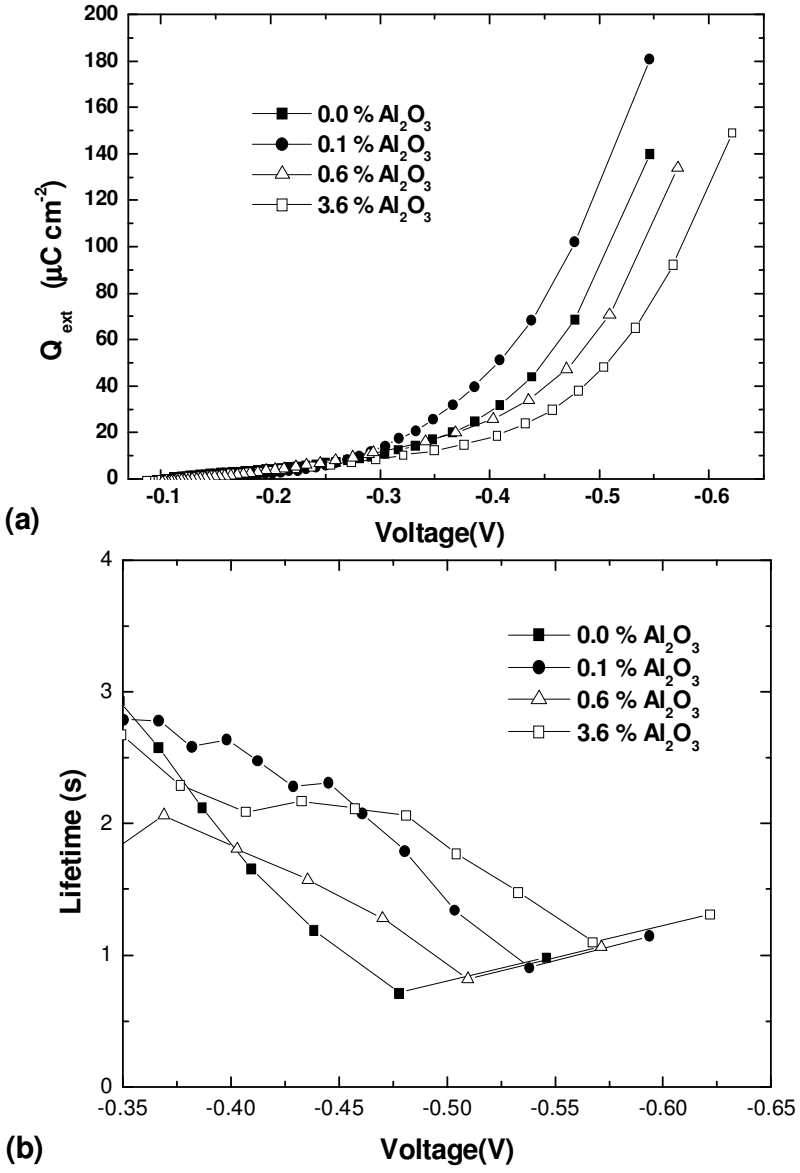

Figure 18. *(a) Extracted charge as function of voltage. (b) Electron lifetime as function of voltage.*

Figure 19a shows τ_{IMPS} as a function of light intensity. The electron transport becomes more rapid with increasing light intensity, as has been observed in previous studies.[49-51] The electron transport times are nearly identical for samples without aluminum oxide and with 0.1 wt. % aluminum oxide, but increases significantly for samples with more aluminum oxide. The slopes of the curves in the double logarithmic plot are very similar (-0.92).

The transport time of the electrons in the nanostructured TiO_2 film is related to the electron concentration in the film. The amount of accumulated electrons was therefore determined using photocurrent transients. Figure 19b shows the extracted charge under short-circuit conditions as a function of light intensity. The general trend is that the charge in the nanostructured TiO_2 increases with light intensity.

The slope in the double logarithmic plot is about 0.43 for all cells. The extracted charge from the solar cell with 0.1 wt.% aluminum oxide is systematically higher than that of the solar cell without aluminum oxide.

Figure 19c shows the electron transport time as a function of the extracted charge. Electron transport becomes faster as more charge is accumulated. Interestingly, all the solar cell with aluminum oxide has an increased electron transport time compared to the blank.

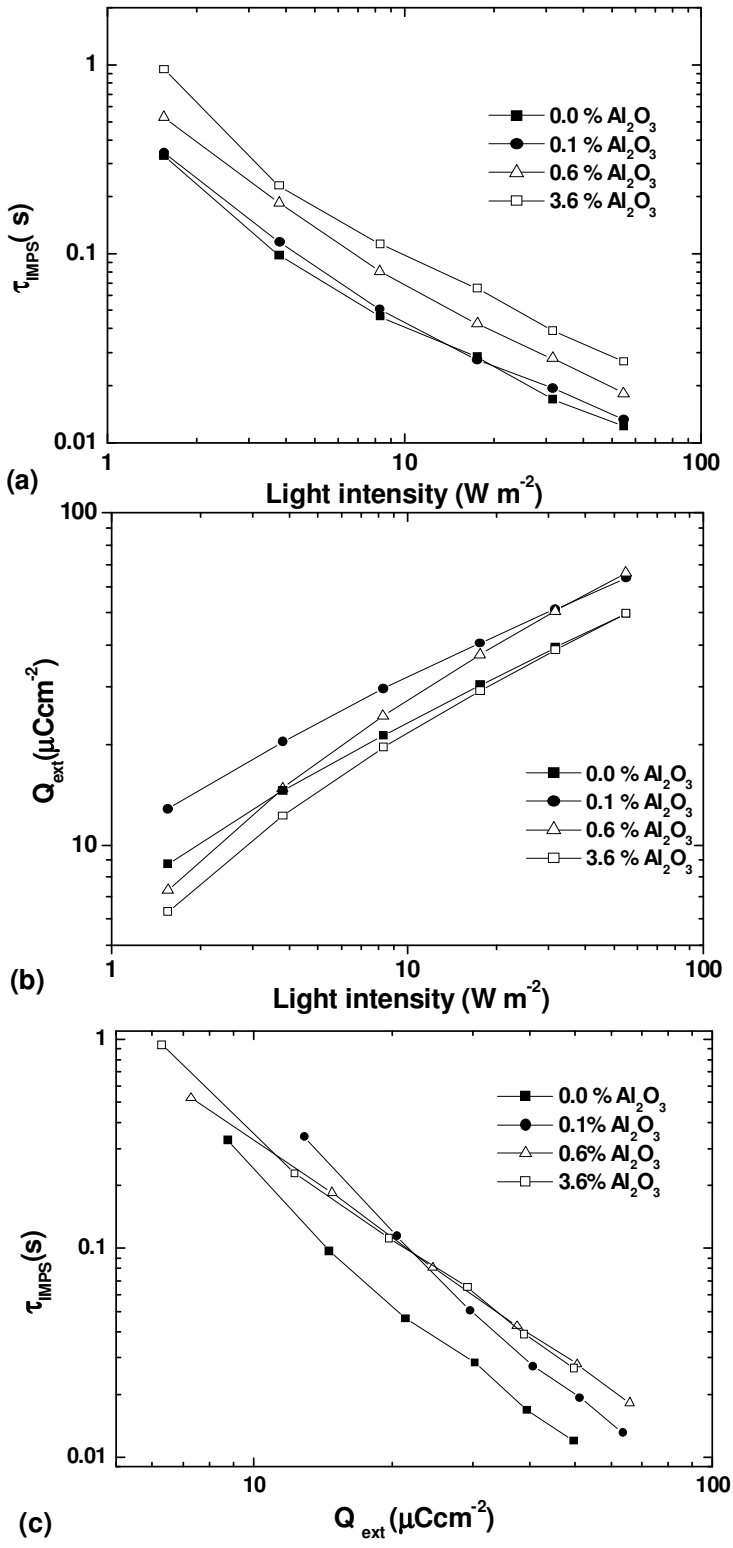

Figure 19. *(a) Electron transport time as function light intensity (b) Extracted charge as function light intensity (c) Electron transport time as function of extracted charge from the solar cell.*

3.2. Results. Method B.

Figure 20 shows a cyclic voltammogram of a nanostructured TiO_2 electrode in 1.0 M $Al(ClO_4)_3$ / polypropylene carbonate. When the potential is scanned in negative direction, a cathodic peak is observed at -1.3 V. In the reverse scan a much smaller anodic peak appears at +0.08V. The cathodic charge is much larger than the anodic one, indicating a largely irreversible electrochemical process. The color of the electrode changed from white to a gray / dark blue color in the first scan to negative potential, and became lighter again at positive potential.

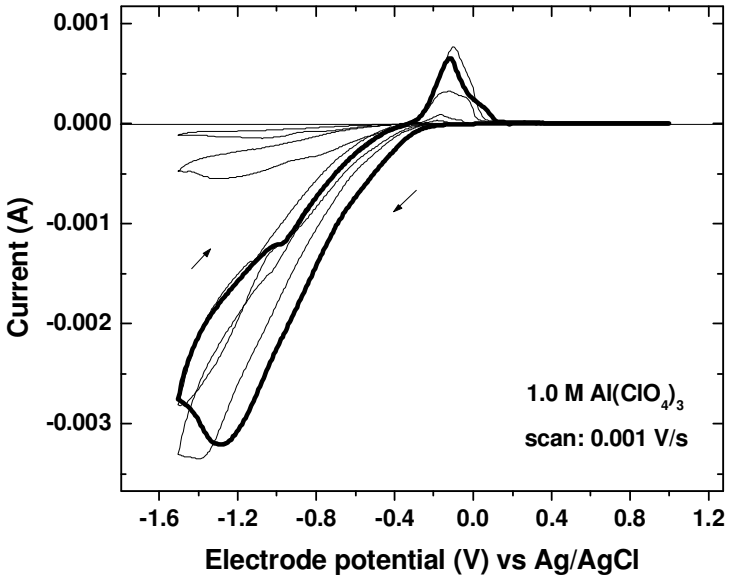

Figure 20. *Cyclic voltammetry of a nanostructured TiO_2 electrode in 1.0 M aluminum perchlorate in polypropylene carbonate, scan rate 1 mVs^{-1}.*

After further cycling, the current decreased much after the third cycle and a gray color was maintained. The fact that the current decreases sharply after a few potential sweeps suggests that the electrode surface is effectively blocked for further reaction. After annealing films became pure white. As will

be shown later, the cathodic process is related to incorporation of aluminum in the TiO_2 film.

Chronoamperometry was used to obtain electrodes with a controlled amount of aluminum, which were used in the solar cells. The potential was stepped to –1.3V and kept at this potential for different periods of time.

Figure 21 shows Raman spectra of the samples that were annealed at different temperatures. The main Raman bands can be attributed to the anatase and rutile phases. The bands at 395, 515, 640 cm^{-1} are attributed to Raman-active modes of anatase phase with symmetries of B_{1g}, B_{1g} and E_g, respectively,[52] while the band at 450 cm^{-1} is ascribed to the E_g modes of rutile phase.[53] A small peak is observed in 936 cm^{-1}. This peak is characteristic of the perchlorate ion.[54]

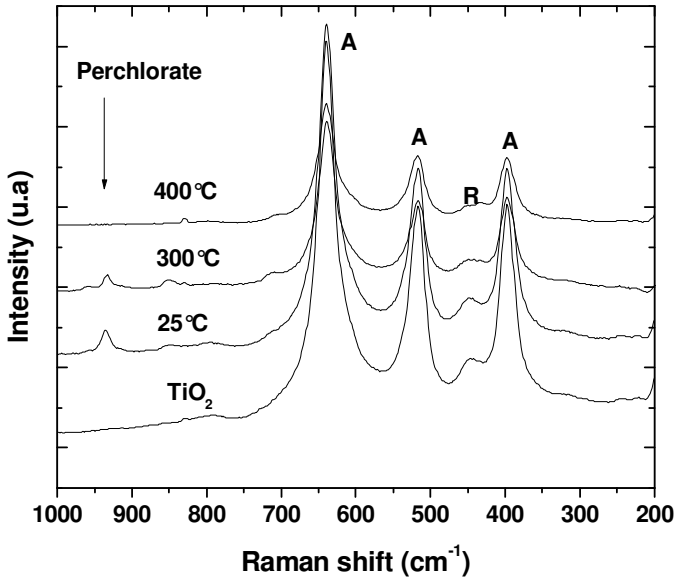

Figure 21. *Raman spectra of TiO_2 electrodes containing aluminum ions, annealed in air at different temperatures. A= anatase, R= rutile*

This peak disappears after heating the electrode to 400°C for 10 min. It was found necessary to anneal the electrodes at 400°C to improve dye adsorption at the electrode. An X-ray diffraction study of the aluminum-modified TiO_2 samples (heated to 400°C) did not reveal any peaks other than those of TiO_2 and SnO_2 (from the substrate).

Neutron activation, analysis clearly demonstrates the presence of aluminum in the samples, see Table 2. The weight percentage of aluminum that was measured in the films shows a good correlation with the cathodic charge in the chronoamperometric deposition process. More specifically, it could be established that three electrons are needed for deposition of one aluminum ion. In the calculations Faraday's law was used, as well as, the porosity of the TiO_2 film of 50%, and the specific density of anatase of 3.8 g/cm^3. The Faradaic efficiency (wt% Al measured / wt% Al calculated from cathodic charge) of the deposition process was calculated to be 84%. Hereafter samples will be indicated by the *calculated* weight percentage of aluminum.

Time at -1.3V(s)	Al/Ti (calc. at. ratio)	TiO_2 wt.% (calc.)	Al wt.% (calc.)	Al wt.% measured (+/- 0.01)
0	0.000	100.00	0.00	0.00
10	0.052	98.29	1.71	1.62
15	0.063	97.91	2.09	1.91
30	0.131	96.34	3.66	3.44
50	0.182	94.25	5.75	4.93
300	0.401	88.20	11.80	9.76

Table 2. *Determination of the amount of aluminum insert into TiO_2 with comparison of the amount calculated from the cathodic charge in chronoamperometric experiment and the measured by Neutron Activation analysis.*

To investigate the composition of Al-modified TiO_2 samples, we report on XAS and PES results for the 11.8 wt% Al sample below. Pure TiO_2 and the Al_2O_3 samples were also investigated and used as a reference. XAS measurements are sensitive towards changes in the local environment of an element.[55]

The Ti2p XAS spectrum of the Al-modified TiO_2 sample was dominated by the anatase crystal structure and possessed the same characteristics of the unmodified TiO_2, see Figure 22. Thus, it can be concluded that there was no formation of an alternative phase, such as aluminum titanate, β-Al_2TiO_5, as a result of the Al-modification.[56]

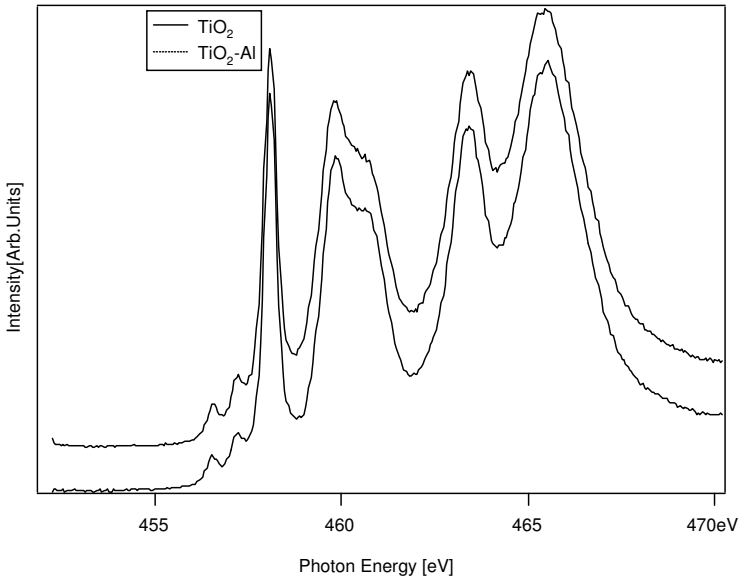

***Figure 22**. Ti2p XAS spectra of TiO_2 and Al-modified TiO_2 films (11.8 wt%Al).*

The results of the core level PES measurements are shown in Figure 23. The substrate $Ti2p_{3/2}$ signal was measured for the TiO_2 and the Al-modified TiO_2 sample (Figure 23b). Comparison of the $Ti2p_{3/2}$ peak for the two samples reveals that the $Ti2p_{3/2}$ peak is damped after Al-modification by 25%. The Al2p spectra are shown in Figure 23c for the Al modified TiO_2 sample and the Al_2O_3 sample. The Al2p signal is build up by spin-orbit split

doublets, $Al2p_{3/2}$ and $Al2p_{1/2}$ (i.e. one doublet peak with an intensity ratio 2:1, and an energy split of 0.4eV), and the signal for the Al modified TiO_2 (Figure 23c) can be fitted reasonably with one such doublet. The Al2p peak in the Al-modified TiO_2 sample is somewhat narrower than in the Al_2O_3 sample.

The O1s PES spectrum of TiO_2 contains two clear contributions (Figure 23a). The peak at lower binding energies is characteristic of oxygen in the TiO_2. The smaller peak at higher binding energies in the TiO_2 sample is attributed to surface adsorbed oxygen contamination (that is water and possibly also oxidized hydrocarbons) due to ex-situ preparation of the samples. In the case of the Al-modified TiO_2 sample there is an increase in intensity of the higher binding energy peak.

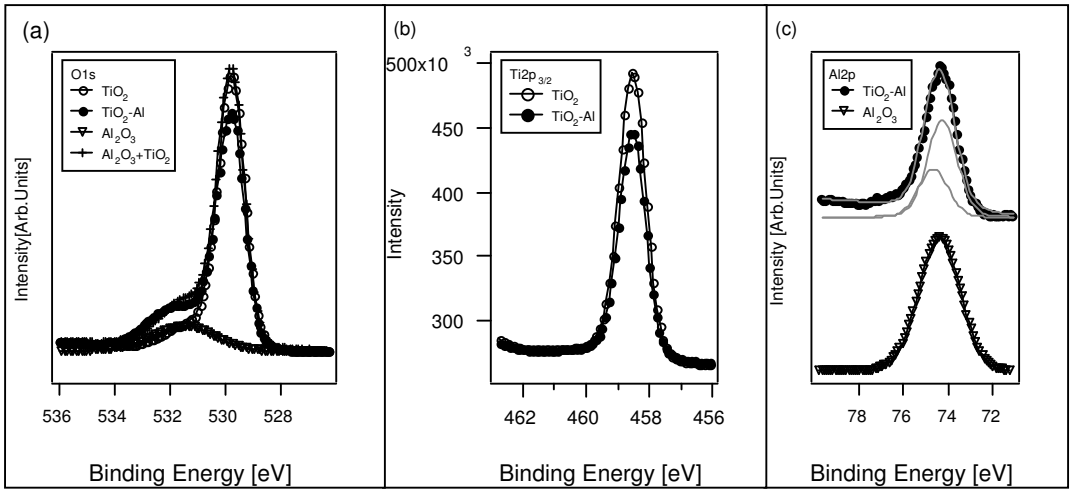

Figure 23. *PES spectra of TiO_2, Al-modified TiO_2 (11.8 wt% Al) and Al_2O_3 films. (a) O1s spectra, (b) Ti2p spectra and (c) Al2p spectra.*

The position of this peak is at the same binding energy as that of oxygen in the Al_2O_3 sample. A convolution of O1s contribution of the TiO_2 and the Al_2O_3 samples is also shown in the O1s spectrum.

The Ti3p peak and the Al2p peak were measured using three different photon energies, 758eV, 454eV and 150eV, and their relative intensities are shown in Table 3. The Al2p peak increases compared to the Ti3p peak when

going to the more surface sensitive mode that is from higher to lower photon energies.

hν	I(Ti3p)	I(Al2p)	σ(Ti3p)	σ(Al2p)	I*(σ(Ti3p)/σ(Al2p))
758	1.00	0.65	0.07	0.07	0.65
454	1.00	2.53	0.2	0.25	2.02
150	1.00	9.39	1	4	2.35

Table 3*.The area of the intensity of the Ti3p and the Al2p peaks for photon energies 758eV, 454eV and 150eV, the cross section for ejection of electrons at different binding energies (σ) and the correction in intensity using the cross section term [a].*

[a] The data were obtained using synchrotron radiation

The binding of catechol at the surface of the Al-modified TiO_2 electrodes was investigated by visible reflectance spectroscopy. Typical reflectance spectra are shown in Figure 24. The Al-modification of the TiO_2 leads to some reduction of the reflectance in the visible region.

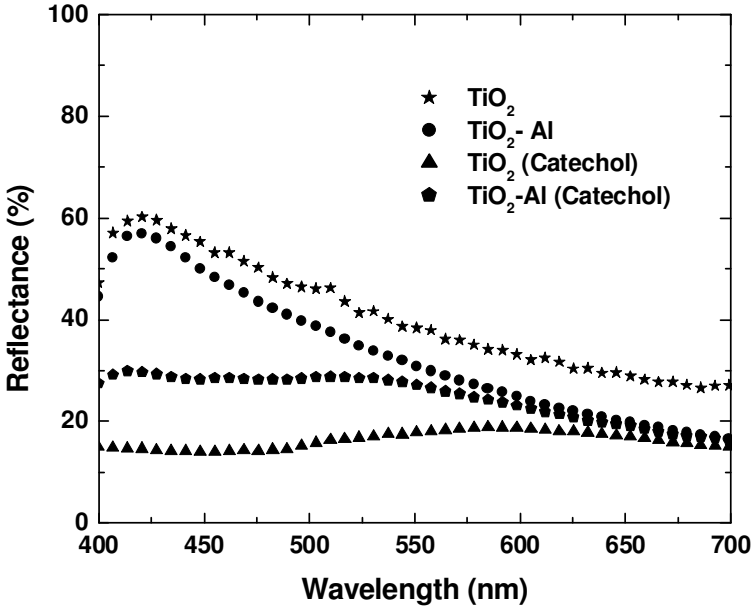

Figure 24. *Total reflectance spectra of TiO_2 and Al-modified TiO_2 films (11.8 wt% Al) with and without adsorbed catechol.*

Brown coloration takes place upon catechol adsorption both in the blank TiO_2 sample and the Al-modified TiO_2, but the degree of coloration

(corresponding to a smaller reduction of the reflectance) is less in case of the Al-modification. This gives further evidence that the aluminum modification does not results in a complete shell of aluminum oxide around the TiO_2 particles, as part of the Ti atoms must still be exposed at the surface.

Figure 25 shows the short circuit current density, J_{sc}, open circuit voltage, V_{oc}, fill factor, *FF*, and the efficiency η, for solar cells with different amounts of aluminum.

The open circuit voltage and the fill factor do not change significantly with the aluminum content of the films: V_{oc} varies between 0.76 and 0.79 V, whereas the *FF* varies between 0.56 and 0.63.

The parameter that governs the behavior of the solar cell efficiency most is the short circuit current. J_{sc} reaches a maximum value for cells prepared with 2 wt% aluminum. Higher aluminum content leads to a decrease in J_{sc} and η. The efficiency for solar cells of TiO_2 with 2.09% Al is 5.6%, while it is 4.4% for the blank sample.

Figure 26 shows the IPCE as a function of illumination wavelength for cells obtained with different amounts of aluminum incorporated in the TiO_2. It is observed that the film with 2.09% of aluminum shows the highest IPCE of 0.53 at 550 nm, while at higher amounts of aluminum (11.8%) the IPCE maximum diminished to 0.25.

The inset in Figure 26 shows normalized IPCE spectra. It demonstrates that some improved IPCE response is found in the 550-700 nm region for the Al-modified samples. It was checked that this effect is not related to the amount of adsorbed dye. Dye desorption experiments, as describe before, showed that the amount of adsorbed N719 dye was not affected by the amount of aluminum. Using molar absorption coefficient for N719 in basic aqueous solution of 12.5×10^3 $M^{-1}cm^{-1}$, the concentration of dye in all samples was found to be 0.12 mmol cm^{-3}.

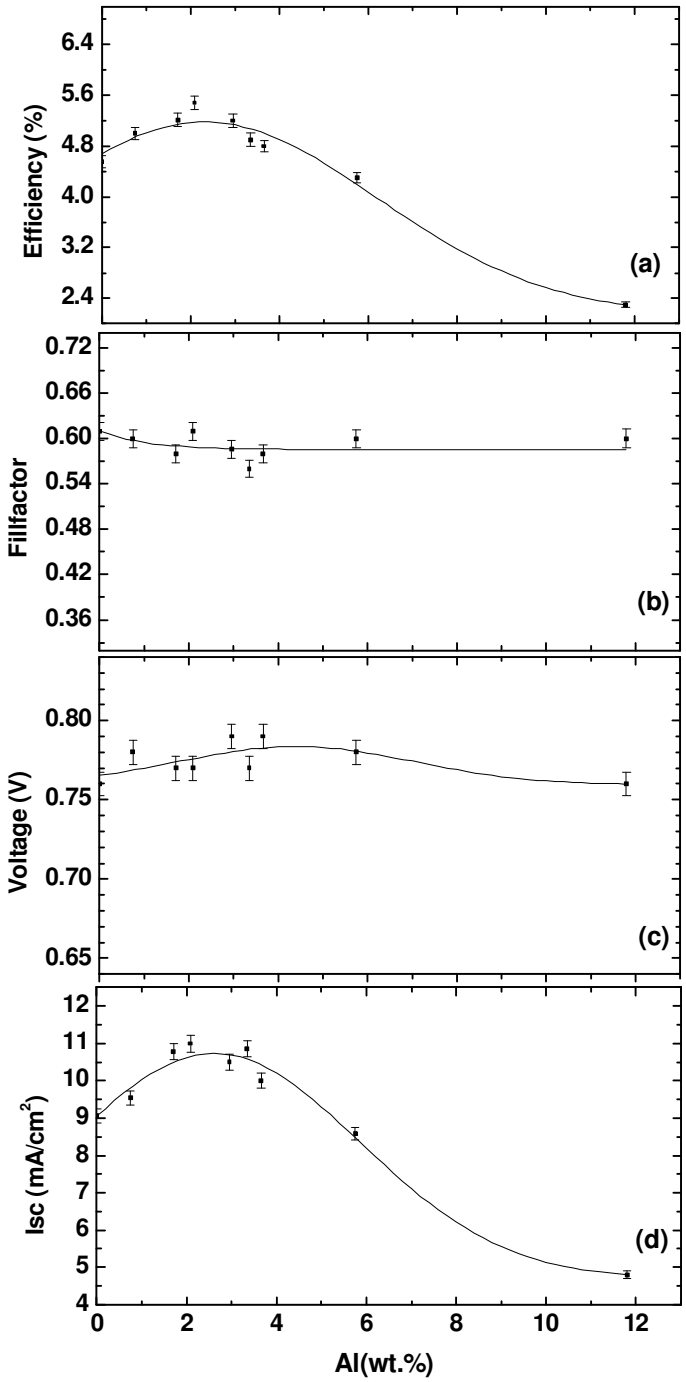

Figure 25. *(a) Efficiency, (b) short circuit current density, (c) fill factor, and (d) open circuit voltage for dye-sensitized solar cells containing different amounts of aluminum. The light intensity during the experiments was equivalent to 1 sun (1000 W m^{-2} with AM 1.5G spectral distribution).*

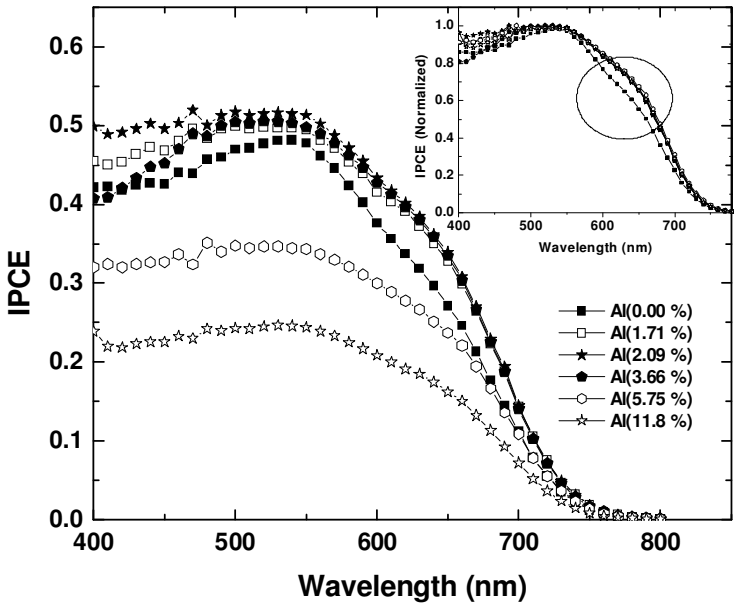

***Figure 26**. IPCE spectra for samples contained at different amount of aluminum ions. The inset shows IPCE spectra normalized at their maxima.*

Figure 27 shows the results of charge extraction experiments on the dye-sensitized solar cell performed at open-circuit potential.[47] A significant effect was found for the Al-modified samples: more charge was extracted at a given voltage. The slopes of the log (charge)-potential plots are quite similar for all samples.

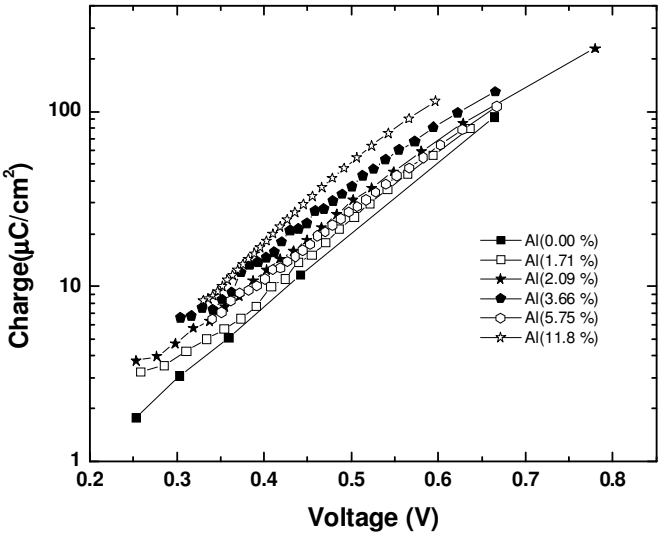

***Figure 27.** Extracted charge as a function of the open-circuit potential in dye sensitized solar cells. The solar cells are prepared with different amount of aluminum ions as indicated.*

Figure 28 shows the electron lifetime (τ_e) as function of the open-circuit potential. The relationship between τ_e and the intensity follows a trend that is generally observed in dye-sensitized solar cells: the lifetime decreases with increasing V_{OC}, following an exponential function.[57] Aluminum-modification of the TiO_2 has a pronounced effect on the electron lifetime: increased lifetimes were found for all Al-modified samples.

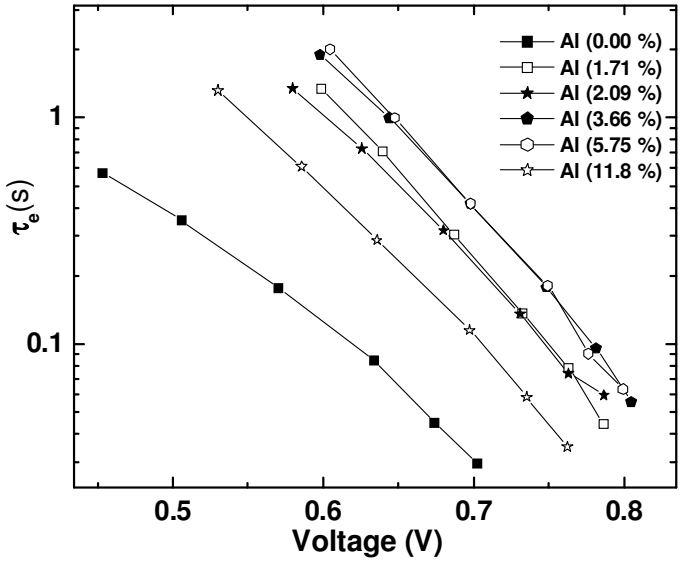

Figure 28. *Electron lifetime (τ_e) as a function of open circuit potential.*

The electron transport time, measured under short-circuit conditions is plotted as a function of the short circuit current density in Figure 29a. An increase of the transport time is found for samples that contained aluminum. The slope of log- log plots of the samples fluctuates between -0.68 to -0.78, while for the blank sample it is –0.57. Figure 29b shows the charge extracted under short circuit conditions as a function of the short circuit current density. Significantly more charge is extracted from aluminum-modified TiO_2 samples than from the blank.

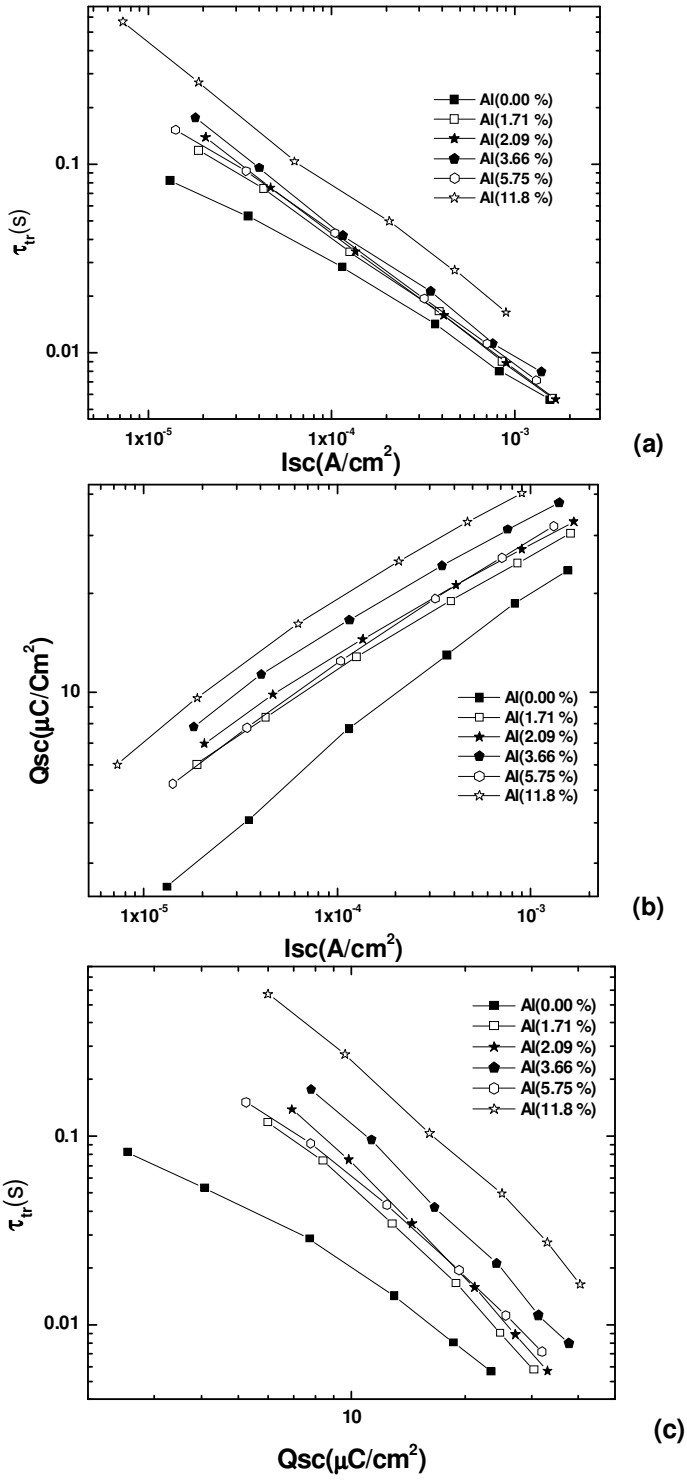

Figure 29. *(a) Electron transport times τ_{tr} as a function of short circuit current density (J_{SC}). (b) The charge in short circuit conditions as a function of J_{SC}. (c) Electron transport time as a function of charge. Time constants were determined using time-resolved small light modulation techniques.*

The slopes in the log-log plot are on average 2.7 for the Al-modified samples, while it was 2.1 for the pure TiO_2. Figure 29c shows the electron transport time as a function of extracted charge. Plotted in this way, the effect of the Al-modification on the transport time is very pronounced: there is one order of magnitude difference in the transport time for the pure TiO_2 and the film with the highest Al-content.

CHAPTER IV

4. Discussion

This chapter have been discussed the main results obtained in this work. The discussion will be divided in two parts:

- About of solar cells made by Method (A)
- About of solar cells made by Method (B)

4.1 About of the solar cells made by Method A.

Aluminum salt treatment of TiO_2 affects the performance of the solar cell in different ways, depending mostly on aluminium concentration, but also, to a small extent on the anion of the salt that was used. $Al(NO_3)_3$ is preferred over $AlCl_3$, as it gives a better overall solar cell efficiency. In what follows we shall discuss only the results obtained for $Al(NO_3)_3$-modified electrodes. From the concentration dependence of the solar cell efficiency we observed an optimum for very small amounts of aluminum oxide, whereas a decrease in efficiency is observed using higher concentrations (Figure 17). The optimum concentration, 0.1wt % of aluminum oxide, is so low that it is insufficient to cover the TiO_2 surface completely. It corresponds to only ~ 4% of full monolayer coverage.

In the following sections, the presented findings shall be rationalized by discussing the effects of the aluminum oxide in terms of band edge movements (energetics), variations in loss reactions, and transport properties (kinetics).

4.1.1. Effects on photovoltage.

The open-circuit photovoltage (V_{OC}) of the solar cell is given by the difference of the quasi-Fermi level of the electrons in the metal oxide and the potential of the counter electrode, which is equal to the redox potential of the electrolyte. The quasi-Fermi level depends on the accumulated charge in the

semiconductor, and will approach the conduction band edge when the concentration of conduction band electrons is high. The potential of the conduction band edge (V_{CB}) depends in general on the surface charge of the metal oxide. Since Al_2O_3 is a more basic oxide than TiO_2, we can expect a negative shift of V_{CB}, in the case of aluminum oxide surface modification.[12]

The following relationship is valid:

$$V_{OC} = V_{CB} - \frac{kT}{q} \ln\left(\frac{n_C}{N_C}\right) \qquad (13)$$

where kT is the thermal energy, q is the elementary charge, n_C is the concentration of electrons in the conduction band, and N_C is the effective density of states in the conduction band. Note that both V_{OC} and V_{CB} are given here with respect to the redox potential of the electrolyte and have negative values.

In Figure 18a open-circuit potentials of aluminum oxide modified TiO_2 solar cells are correlated with the charge present in the nanostructured metal oxide film.

This gives a clear indication of shifts of V_{CB} as a function of the aluminum oxide concentration. For 0.6% and 3.6% aluminum oxide V_{CB} is shifted in the negative direction compared to the blank, as it is expected from the basic nature of aluminum oxide. There is, however, a surprising positive shift of V_{CB} for 0.1% aluminum oxide compared to the standard TiO_2 film. Adsorption of aluminum ions will result in a more positive charge at the TiO_2 electrolyte interface and a positive shift of V_{CB}. During heat treatment, however, one would expect a conversion to aluminum oxide, giving a negative shift instead. Apparently, some of the ion adsorption effect is maintained after the heat treatment. Considering the positive shift of V_{CB} for the 0.1% aluminum oxide solar cell one might expect a decrease in V_{OC} with respect to the blank in the current-voltage characterization (Figures 16 and 17). This is, however, not the case.

From Figure 17 it follows that V_{OC} is slightly more negative for the 0.1% solar cell than for the blank. The reason must be a higher n_C due to either a

better injection of electrons into the metal oxide from the excited dye, or suppression of loss reactions. A detailed investigation of the injection process is beyond the scope of this work. Regarding loss reactions, Figure 18b shows measurements of the lifetime of electrons in the oxide film as a function of voltage. It is clearly observed that the aluminum oxide treatment has a beneficial effect, giving generally higher electron lifetimes. In particular, one notes that the lifetime of the electrons is improved at the working point of the solar cell, which is at about (-0.43 V) as obtained from Figure 16.

As the aluminum oxide content appears to be too small to form a blocking layer, specific suppression of recombination centers by the aluminum ions seems the most likely explanation for this effect. The negative shift of V_{CB} of the 0.6 and 3.6 wt % aluminum oxide solar cells that follows from Figure 18a is translated into a more negative V_{OC} in the current-voltage curves (compared to the blank) for the 0.6% cell, but not for the 3.6% cell. A possible cause is a reduced electron injection in the 3.6% cell, as, will be discussed in more detail below.

4.1.2. Effects on photocurrent.

The overall photocurrent can, besides being measured in a solar simulator, also be calculated by multiplying the IPCE times with the number of photons at a given wavelength under AM 1.5 solar conditions and integrating over the entire spectrum. In the analysis of the effect of aluminum ion surface treatment on the photocurrent IPCE data shall be used for the sake of discussion. The IPCE values can be rationalized by the following relationship:[37]

$$\text{IPCE}(\lambda) = \text{LHE}(\lambda) \times \phi_{inj} \times \eta_c \qquad (14)$$

where LHE(λ) is the light harvesting efficiency, ϕ_{inj} is the quantum yield of charge injection, and η_c is the efficiency of collecting the injected charge at the back contact.

Differences in LHE are not expected to be significant in the present experiments since nanostructured films of equal thickness were used, and

also because since the aluminum modification did not affect dye uptake. In Figure 15c an increase of the IPCE values upon aluminum oxide treatment (0.1%) is observed. This can be interpreted as an improved injection efficiency since there appears to be a positive shift of the V_{CB} by the aluminum ion treatment, (Figure 18a), resulting in an improved overlap of the excited dye orbitals with the conduction band acceptor levels. Furthermore, Figure 18b shows that the aluminum oxide treatment results in longer electron lifetimes, indicating a reduction of loss reactions and a probable increase of the charge collection efficiency. Comparing the IPCE values as a function of aluminum oxide concentration one notes a large decrease in IPCE for the 3.6 wt % sample, see Figure 15a. This is most likely caused by a decrease in the injection efficiency due to a thicker aluminum oxide layer. A careful examination of parts a and b of Figure 15 shows a blue shift of the IPCE spectra for the 0.6% aluminum oxide concentration with respect to the 0.1% samples. This finding seems to confirm, the shifts of V_{CB} as discussed above.

A negative shift of V_{CB} can lead to a decrease of the injection efficiency when the dye is excited with lower energy photons. A similar effect was discussed in detail by Boschloo et al.,[58] who observed a negative shift of V_{CB} upon addition of 4-*tert*butylpyridine to the electrolyte.

The transport of electrons in the nanostructured TiO_2 electrode is affected by the aluminum oxide modification, see Figure 19. The general trends are similar in the investigated solar cells:

The transport time decreases, and the accumulated charge in the nanostructured electrode increases with increasing light intensity. It should be noted that to a certain light intensity results in different fluxes of photoinjected electrons and short-circuit photocurrents, depending on the amount of aluminum oxide present. For a proper comparison of electron transport in the aluminum oxide modified TiO_2 films, it is therefore convenient to relate the electron transport times to the amount of accumulated charge present in the nanostructured film. This relationship is shown in Figure 19c. The effect of the aluminum oxide can be clearly observed in this figure: addition of aluminum

oxide increases τ_{IMPS}. A possible explanation is that aluminium ions will be present at the grain boundaries between the TiO_2 particles. This may result in the formation of a barrier for electron transport, as is indicated in Scheme 3a.

To test this hypothesis, an additional series of solar cells was made. A comparison was made between cells where:

(1) The $Al(NO_3)_3$ was mixed with a suspension of TiO_2 particles followed by pressing and sintering as before and,

(2) A pressed and sintered TiO_2 film was treated with a precise amount of $Al(NO_3)_3$ in ethanol, corresponding to 0.1wt % aluminum oxide as in the first experiment, followed by another heat treatment. The latter treatment avoids the presence of aluminum atoms at grain boundaries between the TiO_2 particles, as shown schematically in Scheme 2b.

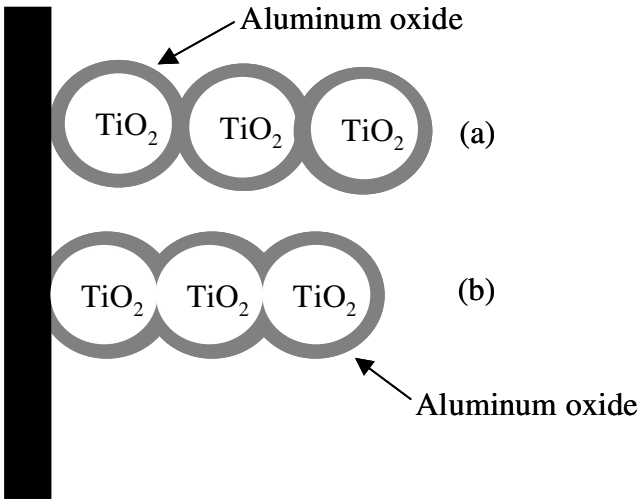

Scheme 3. *Schematic representation of aluminum oxide coated TiO_2 nanoporous films. (a) prepared from a suspension of TiO_2 particles and dissolved $Al(NO_3)_3$ followed by compression and sintering. (b) coating is made on a compressed TiO_2 film.*

The results of transport and charge extraction measurements for this series of solar cells are compared in Figure 30. No significant differences in τ_{IMPS} were found as a function of light intensity (Figure 30a). There are, however, more electrons accumulated under short-circuit conditions in the solar cell where the TiO_2 and $Al(NO_3)_3$ were mixed (Figure 30b). From the plot of τ_{IMPS} vs extracted charge (Figure 30c) it follows that the electron transport is unaffected by the aftertreatment of the nanoporous TiO_2 film with aluminum nitrate, whereas mixing of the aluminum salt with the TiO_2 suspension leads to a reduction of the speed of the electron transport. Considering the very small amounts of aluminum ions used in these experiments, the results should be interpreted with care, but they seem to confirm the hypothesis that aluminum ions present between TiO_2 particles reduce the electron transport speed due to the formation of an energy barrier.

The relatively slow and light-intensity dependent electron transport in nanostructured TiO_2 electrodes is most often explained by using a trapping/detrapping model.[49-51] Traps are localized states with energies below the conduction band edge and located either in the bulk of the semiconductor material, or at the semiconductor/electrolyte interface. Electrons can be captured (trapping) and released after some time by thermal excitation (detrapping). The power-law dependence of the electron transport time and the extracted charge on light intensity can be explained by assuming a trap distribution that increases exponentially towards the conduction band.[50,51] The slope of the trap distribution can be determined from the double logarithmic plots of τ_{IMPS} and extracted charge vs light intensity (Figure 19a,b). It follows from this figure that the slopes do not change significantly with the aluminum oxide coverage. This may be an indication that traps are not located at the semiconductor/electrolyte interface where the aluminum ion treatment is expected to have a large effect. It also appears that the aluminum salt treatment does not create a large amount of additional trap states, as the charge in the film remains quite similar (Figure 19b).

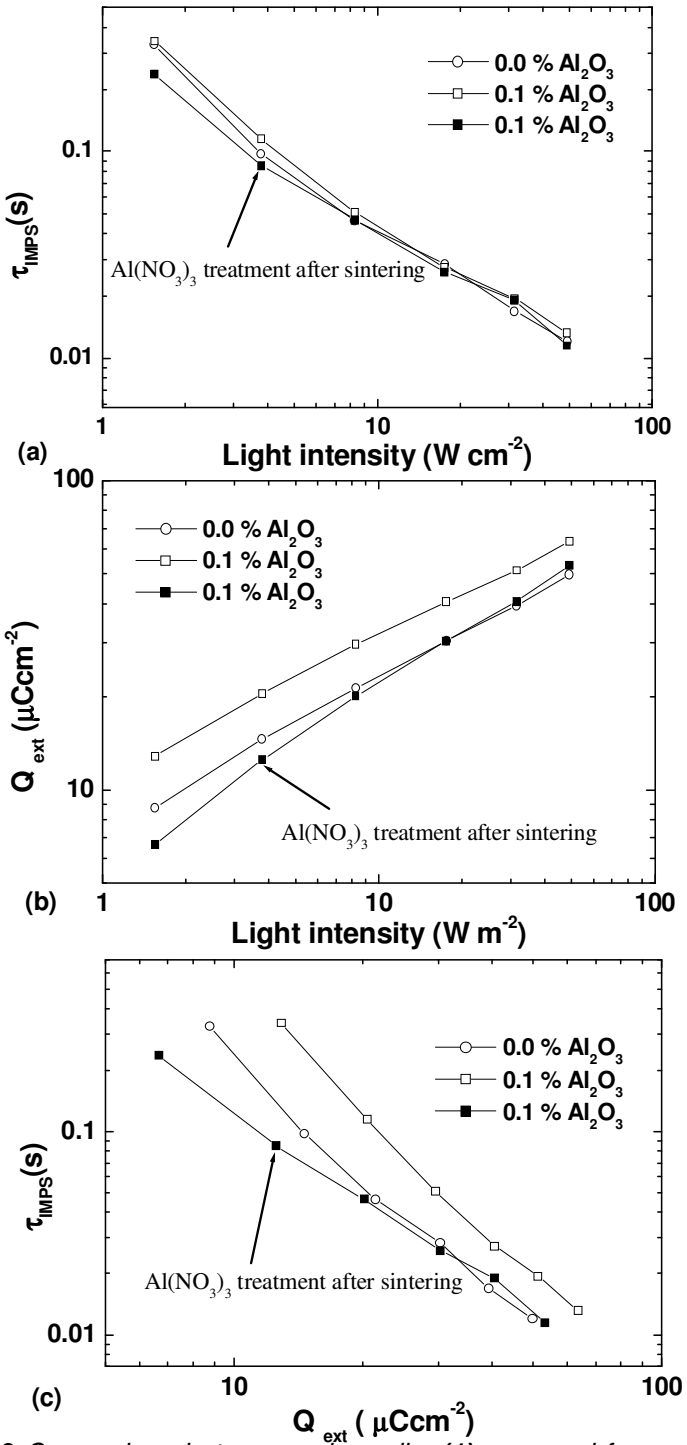

Figure 30. *Comparison between solar cells: **(1)** prepared from a suspension of TiO_2 particles and dissolved $Al(NO_3)_3$ followed by compression and sintering, with 0.0 wt. % aluminum oxide (o) or 0.1 wt.% aluminum oxide ( ), **(2)** a coating of $Al(NO_3)_3$ is made on a compressed TiO_2 film, followed by heating, corresponding to 0.1% wt aluminum oxide(■), (a) Electron transport time as function light intensity (b) Extracted charge as function light intensity (c) Electron transport time as function of extracted charge from the solar cell.*

4.2. About the solar cells made by Method B.

The results of the electrochemical experiments of nanostructured TiO_2 in Al^{3+} containing electrolyte demonstrate that aluminum ions are incorporated in the electrode when sufficiently negative potentials are applied. The precise nature is of the aluminum deposition is not clear. The cyclic voltammogram (Figure 20) resembles that of Li^+ intercalation in TiO_2 to some extent, with the important difference that Li^+ intercalation is much more reversible.[16] The peak current in the cathodic scan was in fact quite similar in Al^{3+} and Li^+ containing electrolytes. Assuming an intercalation process, the overall electrochemical reaction may be written as follows:

$$x\ Al^{3+} + 3x\ e^- + TiO_2 \rightarrow Al_xTiO_2 \qquad (15).$$

The inserted Al^{3+} ions, which have a significantly smaller ionic radius than Li^+ (45 and 68 pm, respectively), require charge compensation by 3 Ti^{3+} atoms in the TiO_2 lattice. Ti^{3+} species are in general responsible for a gray / dark blue coloration in TiO_2. Such coloration was indeed observed. The irreversibility of the electrochemistry suggests that Al_xTiO_2 reacts further with water or oxygen impurities to form $AlO_xH_y.TiO_2$, which will be transformed in a mix of Al_2O_3 and TiO_2 after annealing in air.

In the presence of a substantial amount of water in the electrolyte, the reaction pathway may be different:[15]

$$2\ H_2O + 2e^- \rightarrow 2\ OH^- + H_2 \quad (16a)$$
$$Al^{3+} + 3\ OH^- \rightarrow Al(OH)_3 \quad (16b)$$

After annealing in air, again a mix of Al_2O_3 and TiO_2 will be formed. The difference with reaction 15 is that probably no mixed phase of the two components is formed. As the electrolyte used was not water-free, reaction 16 is a possible mechanism. However, no bubbles that would indicate the

evolution of hydrogen were found. As Ti^{3+} species are appearing in the process, evident from the darkening of the TiO_2 electrode, it is possible that the initial step in reaction 16 involves the intercalation of protons, charge compensated by Ti^{3+} species, rather than direct hydrogen evolution:

$$H_2O + TiO_2 + e^- \rightarrow OH^- + HTiO_2 \quad (16c)$$

The PES measurements of the Ti2p peak, the Ti^{3+} species would appear at the lower binding energy side of the main Ti^{4+} peak. The measured Ti2p (Figure 23b) shows that no noticeable amounts of Ti^{3+} species are present in the sample after the annealing process.

The decrease of the Ti2p peak intensity for the Al modified TiO_2 compared to the TiO_2 sample was 25%. In a model where the aluminum is present as a dense shell of Al_2O_3 covering the surface of TiO_2, it can be calculated that 10 wt% Al would correspond to a 1 nm thick Al_2O_3 layer (the specific area of the nanostructured TiO_2 is 55 m^2/g). Using a mean free path of ~23Å in Al_2O_3 for photons with an energy of 1000eV, such a shell structure is expected to result in a decrease of the XPS intensity of the Ti-peaks by 35%.

Since a smaller value is observed the results indicate that the Al_2O_3 does not form a dense even shell. The results rather suggested that the Al-deposition is not uniform. One explanation is that there is more deposition near the conducting glass substrate. It is likely that part of the electrochemical reaction take place on the SnO_2:F substrate, possibly forming a blocking layer. Another explanation is that Al is inserted into the TiO_2 lattice, or that there is deposition of Al_2O_3 as islands on the surface of TiO_2. The latter explanation is also in agreement with the results of the catechol adsorption study using reflectance spectroscopy.

The PES studies the Al2p peak was clearly observed in the Al modified TiO_2 electrodes, see Figure 23c. This demonstrates that aluminum was also deposited on the outmost part of the TiO_2 film, as 95% of the PES data is

obtained only from the outmost ~6 nm of the film at the photon energies used. Since a reasonable fit of the Al2p signal could be obtained with only one spin-orbit split peak, this suggest that there is only one type of Al dominating the Al structure, possibly as an Al_2O_3 layer.

This is also supported by the O1s measurements. The O1s PES spectrum of the Al-modified TiO_2 sample could be modeled reasonably, with respect to intensity and peak position, as a convolution of contributions from the measured O1s spectra of Al_2O_3 and that of TiO_2, see Figure 23a.

Thus in the O1s spectrum of the Al-modified TiO_2 sample the higher binding energy peak is attributed to oxygen bound to Al. The position of the O1s contribution in the Al-modified TiO_2 sample at the higher binding energy again indicates no formation of aluminum titanate, in accordance with the XAS results.[59]

When the Ti3p peak and the Al2p peak were measured using three different photon energies, 758eV, 454eV and 150eV, the area of the Al2p peak increase compared to the Ti3p peak as the surface sensitivity of the measurements increases, i.e. going from higher to lower photon energies, see Table 3. Introducing corrections for the change in cross-section for the emission of electrons from the different energy levels, σ(Ti3p) and σ(Al2p) do not change the trend of the intensity relationship.

Therefore, it can be concluded that a majority of the Al^{3+} ions are located in the surface region of the nanoparticles.

Adsorption of catechol appears to be a useful method to investigate surface modified TiO_2 electrodes. Catechol forms charge–transfer complexes on TiO_2 surfaces, with a strong brown color (catecholate species in a chelating configuration),[60-62] but can also give molecular adsorption, which is colorless. In the case of aluminum oxide, the catechol adsorption occurs and no color change is observed, due to that the charge-transfer occurs in the UV region.[63] The color change of aluminum-modified titanium dioxide samples upon adsorption of catechol gives therefore information on the atomic composition of the surface.

It is evident from the catechol adsorption experiment (Figure 24) that a significant part of the Ti surface atoms is still exposed at the surface after Al-modification and heat treatment. This suggests that the incorporated aluminum is present either as a non-uniform layer (small particles) of aluminum oxide on the TiO_2 surface. The reduction of the reflectance of the bare samples in the visible region upon Al-modification must be related to a change in the refractive index of the film.

The results of the solar cells prepared from Al-modified TiO_2 films (Figure 25) show that a small but significant improvement of the efficiency, can be obtained by the electrochemical modification. Incorporation of too much aluminum leads, however, to a large decrease in the efficiency as the photocurrent is much decreased. Interestingly, the photocurrent is slightly increased when small amounts of aluminum atoms are incorporated.

This is also apparent in the IPCE spectra (Figure 26), that reveal a modest improvement in the whole IPCE spectrum, but specifically in the 600-700 nm region. There are several possible explanations for this improvement:

(1) A shift of the absorption spectrum of the dye upon adsorption at the Al-modified TiO_2 electrode. Binding of the dye Al-atoms instead of Ti may result in spectral shifts. To test this, N719 dye was adsorbed at transparent nanostructured TiO_2 and Al_2O_3 films. A small blue shift (~5 nm) was observed upon adsorption at Al_2O_3. We can therefore exclude this possibility as an explanation for the improved red response of the in IPCE spectrum.

(2) Improved electron injection efficiency: the injection efficiency from low-lying excited states from the N719 dye may critically depend on the density of isoenergetic acceptor states in TiO_2. Al-modification can affect the position of the conduction band of TiO_2, and thereby the number of available acceptor states. Improved red response in the

IPCE spectrum may occur if the potential of the conduction band edge is shifted to more positive potentials.

(3) A longer diffusion length will result in improved red response, as red photons are on average absorbed further away from the conducting substrate than blue or green ones.[64]

A series of advanced techniques was used to provide more insight on the precise action of the Al-modification. The charge – open circuit potential relationships shown in Figure 27 can be interpreted in two different ways. At a given charge, a higher V_{OC} is observed for the unmodified TiO_2 sample than for the Al-modified ones. This can imply that the conduction band edge (V_{CB}) of TiO_2 shifts to more positive potentials upon Al-modification. This would be in accordance to explanation (2) of the IPCE spectral shift. Interestingly, if we compares this result with the obtained for the Method A, the opposite effect was found: larger V_{OC} was obtained with Al-surface modification (except at the lowest Al-concentration), related to a shift of the TiO_2 conduction band to, more negative potential.

Because aluminum oxide is a more basic oxide than TiO_2, this effect may be explained by the tendency of Al_2O_3 to deprotonate the TiO_2 surface, thereby shifting V_{CB} negatively.[12]

Furthermore, Al_2O_3 has its conduction band edge at more negative potential than TiO_2, so that one would expect a shift to V_{CB} toward more negative potentials in the case of a mixed Al/Ti oxide (compared to pure TiO_2). In the case of the electrochemical Al-modification a positive shift of V_{CB} is observed. A possible explanation is that the aluminum is partially present as bound Al^{+3} ions at the interface, which would shift V_{CB} in a positive direction, as do adsorbed cations such as Li^+.

An alternative interpretation of the observations in Figure 27 is an increase of the density of traps in the electrode upon the Al-modification:

more traps need to be filled to reach the same open- circuit potential. A higher trap density would affect electron transport and recombination.

Longer electron lifetimes at open-circuit conditions are found for Al-modified TiO_2 solar cells (Figure 28). The recombination at a given density of electrons in the TiO_2 electrode is reduced by one order of magnitude upon Al-modification. (See Figure 31)

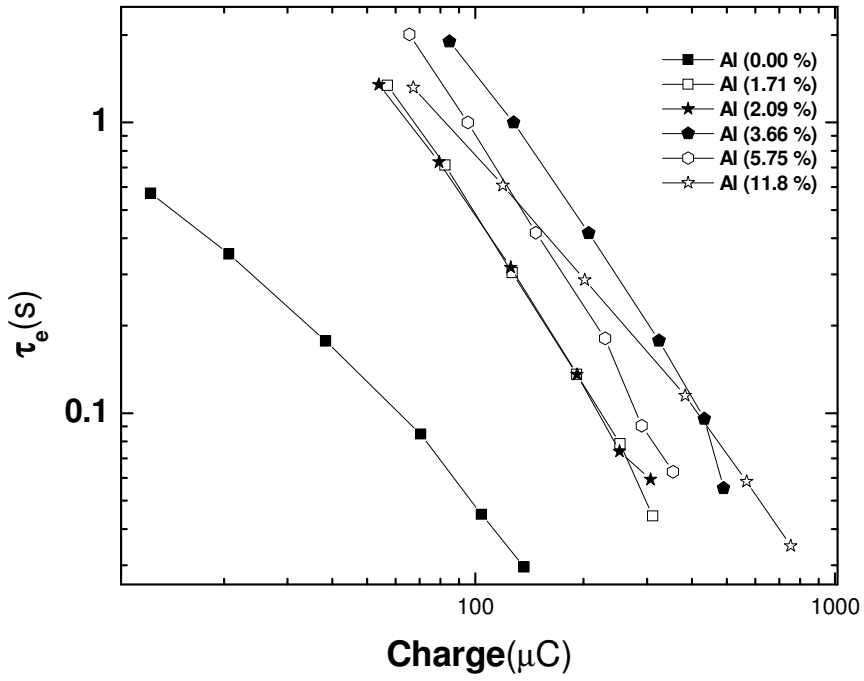

Figure 31. *Electron lifetime as function of extracted charge at open-circuit conditions for Al-modified TiO_2 solar cells.*

If the electrochemical Al-modification creates a higher density of traps, longer lifetimes can be obtained, provided that electrons are mostly trapped and do not recombine from their trapped state, but from conduction band.[65]

Alternatively, the decrease of the rate of electron recombination may be explained by a mixed Al_2O_3-TiO_2 layer or partial aluminum oxide layer that acts as a barrier.

Under operating conditions the electron lifetime will differ significantly from that measured at open circuit.[66] To analyze electron losses at short circuit, relevant for the analysis of the IPCE, τ_e should be determined under short-circuit conditions. One relatively straightforward approach is to measure the internal voltage in the nanostructured electrode under short-circuit conditions,[47] (see Figure 32) and to read out the electron lifetime subsequently from the plot of τ_e vs. V_{OC} (Figure 28).

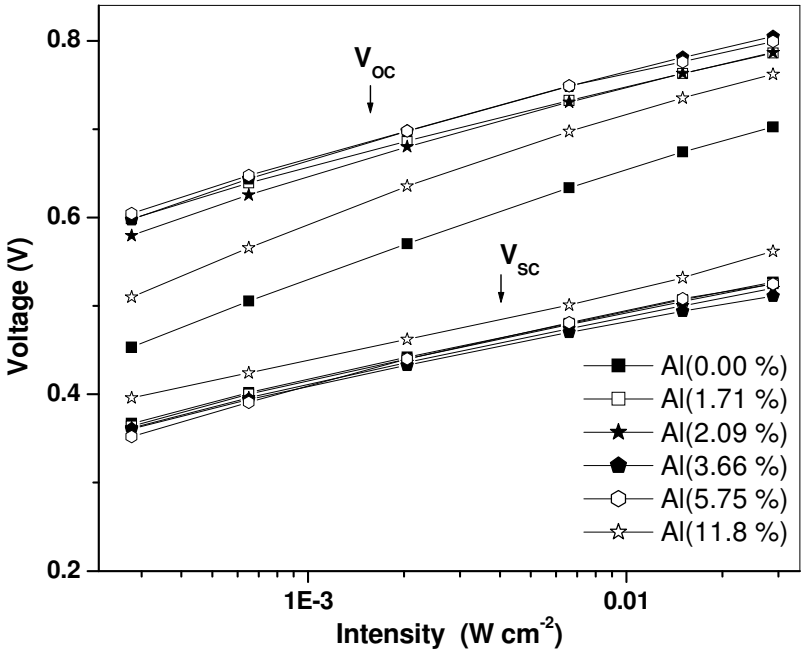

Figure 32. *Open circuit V_{OC} and internal potential in the TiO_2 film under short-circuit conditions V_{SC} as function of monochromatic light intensity (640 nm) VSC was determined by using a switching experiment : The solar cell was illuminated for 5 s under short circuit conditions before, simultaneously, the light was switched off and the cell switched to open circuit. The voltage that develops, referred to as VSC, gives a good indication of the electrochemical potential under short-circuit conditions*

Since the internal voltage under short-circuit conditions is 0.1 - 0.2 V lower than the open-circuit potential found at the same light intensity, the electron lifetime at short circuit ($\tau_{e,SC}$) is about one order of magnitude higher than that at open circuit. The charge collection efficiency at short circuit conditions, which can be calculated using:[50]

$$\eta_c = 1-\tau_{tr}/\tau_e, \quad \text{.....(18)}$$

is therefore very high (>95%). It can be concluded that the significant reduction in the IPCE of the 5.75 and 11.8 wt% Al samples (Figure 25) must be due to a decrease in the electron injection efficiency instead. This may be caused by the presence of either a mixed Al_2O_3·TiO_2 layer (with high band gap), through which tunneling becomes less efficient as the thickness increases, or a partial aluminum oxide layer, where dye molecules adsorbed at Al_2O_3 poorly inject electrons into TiO_2.

Because $\tau_{e,SC}$ is much larger than the photocurrent time response (denoted here as τ_{tr}), it is correct to interpret τ_{tr} directly as the transport time. Transport of electrons through the nanostructured TiO_2 film is clearly affected by the Al-modification: the transport becomes slower upon Al-modification (Figure 29). This could be caused either by an increased density of traps in the TiO_2 due to the Al-modification or possibly by the formation to barrier between the nanocrystals upon the electrochemical Al-modification, both of which would slow down electron transport.

A partial coverage of the TiO_2 by aluminum oxide is not expected to have a significant effect on the electron transport.[13]

Under short-circuit conditions, the calculated diffusion length, given by:

$$L = \sqrt{D \times \tau_{e,SC}}\ , \quad \text{.....(19)}$$

where D is the apparent diffusion coefficient ($D = d^2/(2.35\tau_{tr})$),[67] L is more than 3 times larger than the film thickness d, and is hardly affected by the Al-modification.

Differences in diffusion length have therefore negligible effects on the IPCE spectra. The most likely the explanation for the improved IPCE response (Figure 26) is therefore a positive shift of the conduction band potential.

A multiple trapping model is frequently used to explain the characteristics of transport and recombination in nanostructured TiO_2 solar cells. In general, an exponential distribution of localized states below the conduction band edge is assumed:

$$N_T(E) = N_{T0} \exp\left(\frac{E - E_{F0}}{m}\right) \qquad (20)$$

where N_{T0} is the trap state density at E_{F0}, which is the Fermi-level of the TiO_2 in the dark (equal to the redox energy of the electrolyte), and m is the slope of the trap distribution. The value of m can be derived from different experimental techniques. A summary is shown in Table 4.

The slope of the trap distribution is affected by the Al-modification: m values are about 40 % higher than for the unmodified TiO_2. Another observation is that different experimental methods result in significant differences in the measured m values. Such differences have been observed before.[47]

Experiment	TiO_2 - Al (2.09 %) m (meV)	TiO_2 m (meV)
$\tau_{tr} - J_{SC}$	92	60
Q- J_{SC}	73	54
V– Q	141	103

Table 4. *Parameters of the Multiple Trapping Model with exponential trap distribution (equation 20) obtained for DSSC using different experimental techniques.*

CHAPTER V

5. Conclusions

- Solar cells sensitized prepared using the compression method surface modified with aluminum salt, present a solar efficiency improvement compared to unmodified TiO_2 films. The best performance was obtained with titanium dioxide films modified with a 0.1 wt. % of aluminum oxide using aluminum nitrate. Higher aluminum oxide concentrations generate a reduction of the photoresponse of the solar cells.
- A weight concentration of 0.1% corresponds to less than a monolayer coverage of aluminum oxide. It is therefore not relevant to view the aluminum oxide coating as a layer structure, but as a termination of the TiO_2 surface with Al ions.
- The effects of aluminum salt treatments are to shift potential of the conduction band, to increase of the electron lifetime, and to slower the transport when the aluminum oxide coating is located in between the interconnected TiO_2 particles.
- The addition of aluminum oxide in TiO_2 particles increases the electron transport time, but this treatment does not induce additional trap states. The increase must be due to additional energy barriers in the connection between TiO_2 particles.
- An electrochemical method was developed to incorporate Al^{3+} in nanostructured TiO_2 electrodes. After heat treatment, the resulting electrodes show slightly improved properties in dye-sensitized solar cells.
- Al-incorporation appears to result in a shell of mixed Al -Ti oxide covering the TiO_2 core. This shell works effectively as a barrier for both injection and recombination: When too much Al ions are inserted, the electron injection efficiency from excited dye molecules is decreased.

On the other hand, the recombination of electrons in TiO_2 with triiodide in the electrolyte is reduced upon Al-modification.

CHAPTER VI

6.1 APPENDIX

(A) Model trapping / detrapping.

The rate of electron transport is a major determinant of the overall efficiency of dye-sensitized nanocrystalline TiO_2 solar cells. Following electron injection into the conduction band form optically excited dye molecules, they can traverse the particle network and be collected at the transparent conducting glass back contact, or can react (recombine) with redox species (I_3^-) or dye molecules at particle /electrolyte interface. Usually, the recapture of an electron by the oxidized dye is prevented by an even faster neutralization of oxidized dye by the redox electrolyte (I^-). The collection of electrons competes with the recombination at the nanoparticle/redox electrolyte interface, slow electron transport can lead to a low charge – collection efficiency, and hence to low conversion efficiencies.

The electron transport in nanoporous semiconductor films is assumed to proceed by diffusion because of the absence of a significant electrical potential gradient in the film. The dynamics of the electron- transport process in nanocrystalline TiO_2 films have been studied by intensity modulate photocurrent spectroscopy (IMPS).

Electron transport have been modeled in terms of an effective diffusion coefficient (D_{eff}). This diffusion depends on light intensity.

The IMPS time constant and the short –circuit photocurrent j_{sc} are important parameters for understanding the charge-transport kinetics in dye-sensitized solar cells.

The time constant τ_{IMPS} represents the average time for the collection of injected electrons, and j_{sc} is a measure of the electron-transport rate. The product of τ_{IMPS} times j_{sc} is the number of the electrons Q in the film in the absence of recombination.

Although the underling cause has not been established, the dependence of j_{sc} on Q can be described by a power law; i.e (j_{sc} α Q^m), where m = 2.64. Similarly it can be shown that $\tau_{IMPS} \alpha j_{SC}^{(1/m)-1}$; a double logarithmic plot of τ_{IMPS} vs j_{sc} yields a slope of about – 0.62.

$$\frac{dn_{cb}(x)}{dt} = \alpha\eta_{inj} I(x) + \frac{1}{q}\frac{dj_n(x)}{dx} - U_t(x) + U_e(x) \qquad \text{.....(1)}$$

where at x, n_{CB} is the density of electrons in the conduction band, α is the effective absorption coefficient, η_{inj} is the charge injection efficiency, $I(x)$ is the photon flux or light intensity, q is the unit of charge, and j_n is the electron current density. The first term on the right in the equation (1) is the rate at which electrons are injected into TiO_2 by the excited dye at x.

The second term is the transport component, corresponding to the rate at which electrons, via transport processes, are supplied to x, $U_t(x)$is the rate at which the electrons are capture by traps, Ue(x) is the rate at which electrons are thermally emitted back to the conduction band from the traps. Recombination of electrons from surface states to the redox electrolyte is implicitly contained in the equation (1) as the difference between the terms for electron trapping and emission (detrapping) (Ut – Ue).The electron current density j_n is given by equation:

$$j_n = q\mu_n n_{cb}(\frac{1}{q}\frac{dE_F}{dx}) \qquad (2)$$

where μ_n is the mobility of free electrons, and E_F is the Fermi level, μ_n is limited only by electron scattering at grain boundaries and impurity sites, then it simplifies to:

$$j_n = D_n q\frac{dn_{cb}}{dx} \qquad (3)$$

where D_n is the diffusion constant of free electrons (untrapped) electrons and is calculated form the Einstein equation $D_n = (k_B T / q)\mu_n$; where k_B is the Boltzmann constant and T is the temperature.

As shown by Södergren et al, [64] the solution of the continuity equation can be written in a form that resembles the diode equation describing a conventional p-n photodiode.

$$j = qI_0\left(1 - \eta_{inj} e^{-\alpha d}\right) - q\frac{D_0 n_c^0 d}{L_n^2}\left(e^{\frac{qU}{k_B T}} - 1\right) \qquad (4)$$

The first term in equation (4) corresponds to the light-generated current. It is determined simply by the amount of light absorbed and by the injection efficiency. The second term represents the dark current of the device associated with electron transfer from the TiO_2 to I_3^-. In equation (5), L_n is the diffusion length of electrons in the TiO_2, which is defined as

$$L_n = \sqrt{D_n \tau_n} \qquad (5)$$

where τ_n is the electron life time.

At short circuit, in the absence of recombination (Ut(x)=Ue(x), the steady state free electrons concentration n_{cb} at x can be obtained :

$$n_{cb}(x) = n_{cb}(0) + \frac{n_{inj} I(0)}{\alpha D_n}\left[1 - \alpha x e^{-\alpha d} - e^{-\alpha e}\right] \qquad (6)$$

where the boundary condition of no electron current entering or leaving the TiO_2 film at the outermost TiO_2 /redox electrolyte interfase (Jn(d)=0) is used. The difference between the Fermi level in the dark E_{FO} and under light E_F is calculated from the expression :

$$E_F - E_{FO} = kT \ln \frac{n_{cb}(x)}{n_{cb}(0)} \qquad (7)$$

Intensity –modulated photovoltage spectroscopy indicates that the energy distribution of surface states $N_{ss}(E)$ can be described by a single exponential

$$N_{ss}(E) = N_{sso} e^{(E-E_{FO})/m_c} \quad (8)$$

where N_{ss0} is the surface state density at E_F ,and m_c corresponds to the slope of the surface –state distribution curve.

As the recombination is much slower than trapping and detrapping, the quasi-Fermi level for electrons traps is the same as E_F.

The term quasi Fermi level is used to describe systems in which electrons and holes are in thermal equilibrium with the lattice, but not with each other. This is the situation under steady illumination, where a photostationary state is produced.

OPEN CIRCUIT

Under illumination at open circuit conditions, injection of electrons from photoexcited dye molecules must be balanced by the sum of all routes for electron transfer in the opposite direction. Three such routes can be identified.

The first is the transfer of electrons from the mesoporous TiO_2 layer to I_3^- ions in the electrolyte.[68]

The second is the transfer of electrons from the mesoporous oxide to the oxidised dye molecules attached to the surface, and the third is electron transfer to I_3^- ions via the SnO_2:F back contact. The rate of electron injection is determined by the light intensity and the surface coverage of adsorbed dye. Light scattering can be neglected if the TiO_2 particles are sufficiently small, and the local rate of electron injection $\upsilon_{inj}(\lambda, x)$ can be calculated using the expression for an isotropic non-scattering optical medium,

$$\upsilon_{inj}(\lambda, x) = \eta_{inj}\alpha(\lambda) I_0 e^{-\alpha x} \quad (9)$$

where η_{inj} is the efficiency of electron injection from the excited state of the dye. The absorption coefficient, α, is related to the effective molar concentration *c* and molar absorption coefficient $\varepsilon(\lambda)$ of the dye,

$$\alpha(\lambda) = 2.303\varepsilon(\lambda)c \qquad (10)$$

The rate of reverse electron transfer from the nanocrystalline TiO_2 to the oxidized dye is determined by the competition between reaction

$$D^+ + e^-_{TiO2} \rightarrow D \qquad (11a)$$

and the regeneration step

$$D^+ + I^- \rightarrow D + I^{\cdot} \qquad (11b)$$

Under steady state conditions, the rate of electron transfer to D^+ is given by

$$\upsilon_{D^+} = \upsilon_{inj}\left(\frac{k_{D^+}n}{k_{D^+}n + k_{reg}\left[I^-\right]}\right) \qquad (12)$$

The concentration of iodide ions in the DSSC is usually sufficiently high (> 10^{20} cm^{-3}) and reaction 11a can be neglected to a first approximation.

The rate of electron transfer to I_3^- ions is the dominant quantity that determines the open circuit voltage at high intensities, i.e about 1 sun. In the absence of dissociative chemisorption of iodine, the first step in the reduction

$$I_3^- + e^-_{TiO2} \rightarrow I^- + I_2^{\cdot} \qquad (13a)$$

can be followed either by a second electron transfer step

$$I_2^{\cdot} + e^-_{TiO2} \rightarrow 2\,I^- \qquad (13b)$$

or by the reaction

$$2\,I_2^{\cdot} \rightarrow I_3^- + I^- \qquad (13c)$$

If the step 13a is rate-determining, the expression for the rate of 'recombination' takes the form[69],

$$\upsilon_{I_3^-} = k_{I_3^-}n\left[I_3^-\right] \qquad (14)$$

This rate expression will also be valid if the mechanism involves dissociation of I_2 prior to electron transfer,[70] with the rate constant incorporating the equilibrium constant for dissociation.

The third route by which electrons can react involves transfer from the SnO_2(F) substrate to I_3^-. We can treat this as an electrochemical process using Butler Volmer kinetics.[71] The driving force for the reaction comes from the overpotential – the difference between the potential of an electrode and its equilibrium (Nernstian) potential. In the open circuit case, the potential of the SnO_2(F) electrode is changed under illumination by an amount corresponding to the open circuit voltage. In the dark, the electrode potential is equal to the equilibrium potential of the I_3^-/I^- couple, so the magnitude of the overvoltage under illumination is equal to the photovoltage. The current density associated with reaction 13a can therefore be written as:[72,73]

$$j_{sub} = j_{sub}^{0}\left[\exp\left(\frac{-(1-\alpha)qU_{photo}}{k_BT}\right) - \exp\left(\frac{\alpha qU_{photo}}{k_BT}\right)\right] \qquad (15)$$

(Note that a reduction current is taken to have a negative sign, whereas the photovoltage is taken as a positive quantity). Here, j_{sub}^{0} is the exchange current density, which depends on the standard rate constant for electron transfer k^0 and the concentrations of the redox components.[71]The key point here is that additional current flows internally via the substrate, even though the cell is at open circuit.

The open circuit condition can now be defined in terms of the injection rate and the recombination rates for all three routes using the equivalence

$$\upsilon_{inj} = \upsilon_{D^+} + \upsilon_{I_3^-} - \frac{j_{sub}\left(U_{photo}\right)}{qd} \qquad (16)$$

where d is the thickness of the film.

In order to simplify the treatment at this point, we assume that electron transfer to D^+ and electron transfer via the substrate can both be neglected. For homogeneous illumination, the injection rate is constant over the film and the steady state electron density is given by

$$n = \frac{\upsilon_{inj}}{k_{I_3^-}\left[I_3^-\right]} = \upsilon_{inj}\tau_n \qquad (17)$$

where τ_n is the electron lifetime. It can be seen that this simple approach predicts that the steady state electron density is linearly proportional to the illumination intensity and to the electron lifetime. One way to increase the open circuit voltage is to decrease the concentration of I_3^-. However, this will impose restrictions on the maximum (diffusion limited) current that the cell can deliver. The alternative is to reduce the rate constant for electron transfer by modification of the surface of the TiO_2 particles with blocking layers.[12]

CHAPTER VII

7. REFERENCES

(1) Grätzel, M. *C. R. Chim.* **2006**, *9*, 578.

(2) Kroon, J. M.; Bakker, N. J.; Smit, H. J. P.; Liska, P.; Thampi, K.R.; Wang, P.; Zakeeruddin, S. M.; Grätzel, M.; Hinsch, A.; Hore, S.; Würfel,U.; Sastrawan, R.; Durrant, J. R.; Palomares, E.; Petterson, H.; Gruszecki,T.; Walter, J.; Skupien, K.; Tulloch, G. E. Prog. PhotoVoltaics: Res. Appl. **2006**,15,1,1-18

(3) O'Regan, B.; Grätzel, M. Nature **1991**, 353, 737

(4) Hagfeldt, A.; Grätzel, M. Chem. ReV. **1995**, 95, 49

(5) Hagfeldt, A.; Grätzel, M. Acc. Chem. Res. **2000**, 33, 269.

(6) Lindström, H.; Holmberg, A.; Magnusson, E.; Lindquist, S.-E.;Malmqvist, L.; Hagfeldt, A. Nano Lett. **2001**, 1, 97

(7) Lindström, H.; Holmberg, A.; Magnusson, E.; Malmqvist, L.; Hagfeldt, A. J. Photochem. Photobiol. A: Chem. **2001**, 145, 107.

(8) Tennakone, K.; Kottegoda, I. R. M.; De Silva, L. A. A.; Perera, V. P. S. Semicond. Sci. Technol. **1999**, 14, 975.

(9) Zaban, A.; Chen, S. G.; Chappel, S.; Gregg, B. A. Chem. Commun. (Cambridge) **2000**, 2231

(10) Kumara, G. R. R. A.; Tennakone, K.; Perera, V. P. S.; Konno, A.;Kaneko, S.; Okuya, M. J. Phys. D: Appl. Phys. **2001**, 34, 868

(11) Kay, A.; Grätzel, M. Chem. Mater. **2002**, 14, 2930

(12) Palomares E.; Clifford, J. N.; Haque, S. A.; Luz, T.; Durrant, J. R.J. Am. Chem. Soc. **2003**, 125, 475.

(13) Alarcón, H.; Boschloo, G.; Mendoza, P.; Solis, J. L.; Hagfeldt, A. J. Phys. Chem. B **2005**, 109,18483.

(14) Nanu, M.; Schoonman, J.; Goossens, A. AdV. Mater. **2004**, 16 (5),453.

(15) Yum, J.-H.; Nakade, S.; Kim, D.-Y.; Yanagida, S. J. Phys. Chem.B **2006**, 110, 3215.

(16) Lindström, H.; Södergren, S.; Solbrand, A.; Rensmo, H.; Hjelm,J.; Hagfeldt, A.; Lindquist, S.-E. J. Phys. Chem. B **1997**, 101, 7717.

(17) Lindström, H.; Södergren, S.; Solbrand, A.; Rensmo, H.; Hjelm,J.; Hagfeldt, A.; Lindquist, S.-E. J. Phys. Chem. B **1997**, 101, 7710.

(18) Kopidakis, N.; Benkstein, K. D.; van de Lagemaat, J.; Frank, A. J.,J. Phys. Chem. B **2003**, 107, 11307

(19) Grätzel, M. C. R. Chim. **2006**, 9, 578.

(20) Peter L.M. J. Phys. Chem. C **2007**, 111, 6601

(21) A. Fahmi and C. Minot, Phys. Rev. B **1993**, 47,11717

(22) M.M. Gomez, PhD thesis in Facultad de Ciencias, Universidad Nacional de Ingenieria, Lima , **2001**

(23) W.Kern and E. Tracy, RCA Rev. **1980**, 41, 132

(24) V.Guidi, M. C. Carrotta, M.Ferroni, G.Martinelli, L. Plaglialonga, E. Comini, and G. Sberveglieri, Sensors and Acuators B; **1999**, 57, 197

(25) A. Mills and S.L. Hunte, J. Photobiol. A: Chem . **1997**,108,1

(26) J. Rodriguez, PhD thesis in Facultad de Ciencias, Universidad Nacional de Ingenieria, Lima , **2000**

(27) Wolfbauer, G.,. Bond Alan M,. Eklund John C and Douglas R. MacFarlane, Solar Energy Materials & Solar Cells, **2001**,70, 85-101

(28) Anders Hagfeldt, Bengt Didriksson, Tommy Palmqvist, Henrik Lindström, Sven Södergren, Håkan Rensmo and Sten-Eric Lindquist, Solar Energy Materials and Solar Cells,**1994**, 31, 4, 481-488.

(29) Stanley A., Verity B. and Matthews D., Solar Energy Materials & Solar Cells, **1998**,52, 141-154

(30) Ferber, J., et al., , Investigation of the long-term stability of dye-sensitized solar cells,Proceedings of the 12th Workshop on Quantum Solar Energy Conversion - (QUANTSOL 2000),March 11-18, **2000**, Wolkenstein, Südtirol, Italy

(31) Rijnberg, E., et al., , Long term stability of nanocrystalline dye-sensitized solar cells, 2nd World. Conference and Exhibition on Photovoltaic Solar Energy Conversion, 6-10 July Vienna Austria,**1998**

(32) Kohle O, Grätzel M., F. Meyer, B. Meyer , Adv. Mater., **1997**,9, 11,904-6

(33) Kay, A., Grätzel, M., , Solar Energy Materials & Solar Cells, **1996**,44, 99-117

(34) Smestad, G., et al., , Solar Energy Materials & Solar Cells, **1994**, 32, 3, 259-272

(35) Finnie, K.S.; Bartlett, J.R.; Woolfrey, J.L. Langmuir **1998**, 14, 2744.

(36) Duffy, N.W.; Dobson, K.D.; Gordon, K.C.; Robinson, B.H.; McQuillan, A.J.Chem. Phys. Lett. **1997**, 266, 451.

(37) Nazeeruddin, M.K.; Kay, A.; Rodicio, I.; Humphry-Baker, R;. Müller, E.; Liska, P.; Vlachopoulos, N.; Grätzel, M. J. Am. Chem. Soc. **1993**, 115, 6382.

(38) Rensmo, H.; Södergren, S.; Patthey, L.; Westermark, K.; Vayssieres,L.; Kohle, O.; Brühwiler, P.A.; Hagfeldt, A.; Siegbahn, H. Chem. Phys. Lett.**1997**, 274, 51.

(39) Murakoshi, K.; Kano, G.; Wada, Y.; Yanagida, S.; Miyazaki, H.; Matsumoto,M.; Murasawa, S. J. Electroanal. Chem. **1995**, 396, 27

(40) Zaban, A., Meier, A.; Gregg, B. A. , J. Phys. Chem. B, **1997**,101, 7985-90

(41) Hague S. A., Tachibana, Y.; Klug, D. R.; Durrant, J. R. , J. Phys. Chem. B, **1998**, 102, 1745-1749

(42) Atkins P. and de Paula J. Physical Chemistry, seventh edition, Oxford University press 2002,

(43) De Corte, F. Habilitation Thesis, Ghent University, Faculty of Sciences, Belgium, **1987**

(44) Montoya, E. H.; Cohen, I. M.; Mendoza, P.; Torres, B.; Bedregal, P. J. Radioanal. Nucl. Chem. **1999**, 240, 475

(45) Högdahl In Radiochemical Methods of Analysis: IAEA: Vienna.**1965**; Vol. 1, p 23

(46) Duffy, N. W.; Peter, L. M.; Rajapakse, R. M. G.; Wijayantha, K.G. U. Electrochem. Commun. **2000**, 2, 658

(47) Boschloo, G.; Hagfeldt A. J. Phys. Chem. B **2005**, 109, 12093-12098.

(48) van de Lagemaat, J.; Park, N.-G.; Frank, A. J. J. Phys. Chem. B, **2000**, 104, 2044.

(49) Dloczik, L.; Ileperuma, O.; Lauermann, I.; Peter, L.; Ponomarev, E.;Redmond, G.; Shaw, N.; Uhlendorf, I. J. Phys. Chem. B **1997**,101, 10281.

(50) van de Lagemaat, J.; Frank, A. J. J. Phys. Chem. B **2000**, 104, 4292.

(51) Fisher, A. C.; Peter, L. M.; Ponomarev, E. A.; Walker, A. B.; Wijayantha, K. G. U. J. Phys. Chem. B **2000**, 104, 949.

(52) Ohsaka, T.; Izumi, F.; Fujiki, Y. J. Raman Spectrosc. **1978**, 7, 321.

(53) Chaves, A.; Katiyan, K. S.; Porto, S. P. S. Phys. ReV. **1974**, 10, 3522.

(54) Wang, W.; Ruan, C.; Gu, B. Anal. Chim. Acta **2006**, 567, 121-126.

(55) Stöhr, J. NEXAFS Spectroscopy; Springer-Verlag: Berlin Heidelberg, **1992**.

(56) Soriano, L.; Abbate, M.; Fernandez, A.; GonzalezElipe, A. R.; Sanz,J. M. Surf. Interface Anal. **1997**, 25, 804

(57) Schlichthörl, G.; Huang, S. Y.; Sprague, J.; Frank, A.; J. Phys.Chem. B **1997**, 101, 8141.

(58) Bolso, G.; Lindström, H. ; Magnusson, E.; Holmberg, A.; Hagfeldt, A. J. Photochem. Photobiol. A: Chem. 2002,148,11

(59) Arranz, A.; Palacio, C. ; J. Phys. Chem. B **2002**, 106, 9590.

(60) Rodriguez, R.; Blesa, M. A.; Regazzoni, A. E.; J. Colloid Interface Sci. **1996**, 177, 122.

(61) Liu, Y.; Dadap, J. I.; Zimdars, D.; Eisenthal, K. B.; J. Phys. Chem.B **1999**, 103, 2480.

(62) Lana-Villarreal, T.; Rodes, A.; Perez, J. M.; Gomez, R. J. Am.Chem. Soc. **2005**, 127, 12601

(63) Kummert, R.; Stumm, W. J. Colloid Interface Sci. **1980**, 75, 373.

(64) Södergren, S.; Hagfeldt, A.; Olsson, J.; Lindquist, S.-E.; J. Phys.Chem. **1994**, 98, 5552.

(65) Bisquert, J.; Vikhrenko, V. S.; J. Phys. Chem. B **2004**, 2313

(66) Nissfolk, J.; Fredin, K.; Hagfeldt, A.; Boschloo, G. J. Phys. Chem.B **2006**, 110, 17715.

(67) van de Lagemaat, J.; Frank, A. J. J. Phys. Chem. B **2001**,11194

(68) M. Zukalova, A. Zukal, L. Kavan, M. K. Nazeeruddin, P. Liska and M. Grätzel, Nano Lett., **2005**, 5, 1789-1792

(69) M. D. Wei, Y. Konishi, H. S. Zhou, M. Yanagida, H. Sugihara and H. Arakawa, *J. Mater. Chem.*, 2006, **16**, 1287-1293

(70) A. N. M. Green, R. E. Chandler, S. A. Haque, J. Nelson and J. R. Durrant, J. Phys. Chem. B, 2005, **109**, 142-150.

(71) A. J. Bard and L. R. Faulkner, Electrochemical Methods: Fundamentals and Applications, 2nd edn., John Wiley and Sons Inc, New York, 2001.

(72) P. J. Cameron, L. M. Peter and S. Hore, J. Phys. Chem. B, 2005, **109**, 930-936

(73) P. J. Cameron and L. M. Peter, J. Phys. Chem. B, 2005, **109**, 7392-7398